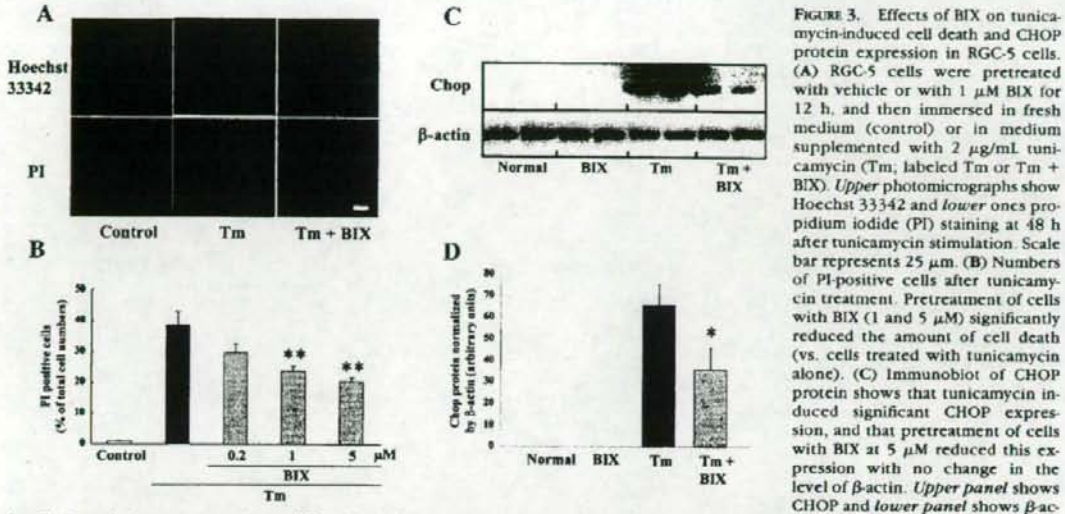

FIGURE 3. Effects of BIX on tunicamycin-induced cell death and CHOP protein expression in RGC-5 cells. (**A**) RGC-5 cells were pretreated with vehicle or with 1 μM BIX for 12 h, and then immersed in fresh medium (control) or in medium supplemented with 2 μg/mL tunicamycin (Tm; labeled Tm or Tm + BIX). *Upper* photomicrographs show Hoechst 33342 and *lower* ones propidium iodide (PI) staining at 48 h after tunicamycin stimulation. Scale bar represents 25 μm. (**B**) Numbers of PI-positive cells after tunicamycin treatment. Pretreatment of cells with BIX (1 and 5 μM) significantly reduced the amount of cell death (vs. cells treated with tunicamycin alone). (**C**) Immunoblot of CHOP protein shows that tunicamycin induced significant CHOP expression, and that pretreatment of cells with BIX at 5 μM reduced this expression with no change in the level of β-actin. *Upper panel* shows CHOP and *lower panel* shows β-actin. (**D**) Quantitative representations of β-actin-based tunicamycin-induced CHOP protein expression (in arbitrary units). Data are shown as mean ± SE (n = 6 or 8). $^*P < 0.05$, $^{**}P < 0.01$ versus tunicamycin alone.

hand, tunicamycin markedly induced CHOP protein, while pretreatment with BIX at 5 μM reduced this expression to almost half the value seen after tunicamycin treatment alone (Figs. 3C, 3D).

Effects of BIX on Cell Damage Induced by Staurosporine in RGC-5 Culture

To investigate whether BIX protects non-ER stress-induced cell death, we examined staurosporine-induced cell death. Staurosporine at 30 nM for 24 h reduced cell viability to approximately 60% of control (Fig. 4). There was no statistical difference between BIX (1 and 5 μM)-treated and vehicle-treated group.

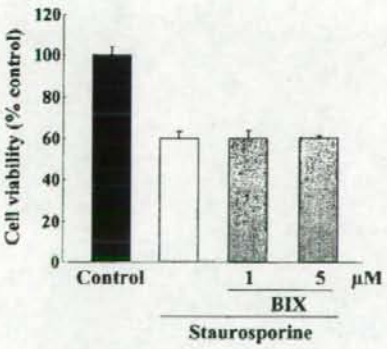

FIGURE 4. Effect of BIX on the cell death induced by staurosporine in RGC-5. RGC-5 cells were pretreated with vehicle or with BIX (1 or 5 μM) for 12 h, and then immersed in fresh medium (control) or in medium supplemented with staurosporine at 30 nM. At the end of this culture period, cell death was assessed by WST-8 assay (Cell Counting Kit-8; Dojin Kagaku). Data are shown as mean ± SE (n = 6).

BiP Protein in the Mouse Retina Induced by Intravitreous Injection of BIX

Compared with that in the nontreated retina, BiP protein expression in GCL and IPL was significantly increased at 6 and 12 h after intravitreal injection of BIX (5 nmol; Figs. 5A, 5B). Optical density analysis confirmed that administration of BIX induced BiP protein in vivo (Fig. 5D).

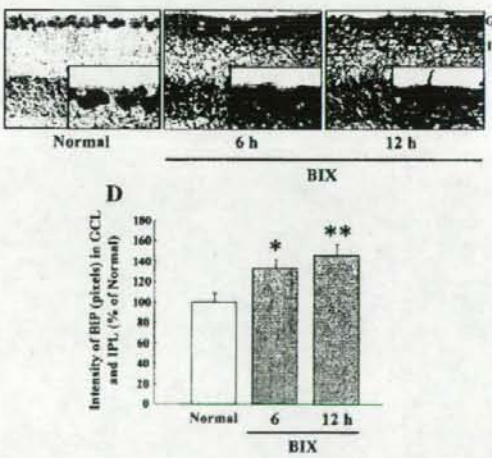

FIGURE 5. BiP protein expression in the mouse retina induced by intravitreous injection of BIX. Immunostaining probed with an antibody against BiP/GRP78. (**A**) Nontreated, (**B**) 6 h, and (**C**) 12 h after intravitreous injection of BIX (5 nmol). (**D**) Expression ratio for BiP induction intravitreous injection of BIX is represented as the ratio of intensity values. Data are shown as mean ± SE (n = 6). $^*P < 0.05$, $^{**}P < 0.01$ versus nontreated normal retina. Each scale bar represents 25 μm.

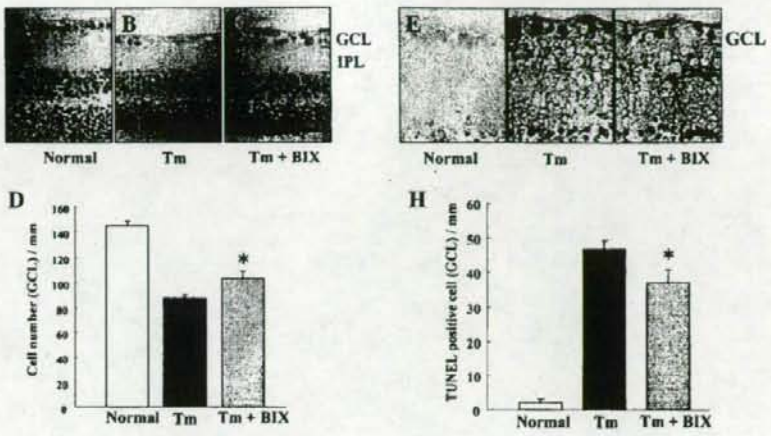

FIGURE 6. Effects of BIX on retinal damage induced by intravitreal injection of tunicamycin in mice. Hematoxylin and eosin staining of cross-sections of (A) nontreated, (B) Tm-treated, and (C) Tm plus BIX-treated mouse retinas at seven days after intravitreal injection of tunicamycin (1 μg) either alone or with BIX (5 nmol). (D) Damage was evaluated by counting cell numbers in GCL at seven days after the above injections. TUNEL staining of cross-sections of (E) nontreated, (F) Tm-treated, and (G) Tm plus BIX-treated mouse retinas at seven days after the above injections. (H) Effect of BIX on Tm-induced expression of TUNEL-positive cells at 24 h after the above injections. Data are shown as mean ± SE (n = 9 or 10). *$P < 0.05$ versus tunicamycin alone. Scale bars each represent 25 μm.

Protective Effect of BIX against Tunicamycin-Induced Retinal Damage in Mice

Tunicamycin decreased the cell number in GCL at 7 days after its intravitreal injection (vs. nontreated retinas; Figs. 6A, 6B). There was significantly less cell loss in GCL when BIX (5 nmol) was co-administered with the tunicamycin (Figs. 6B–6D). In addition, intravitreal injection of tunicamycin increased the number of TUNEL-positive cells in GCL at 24 h (vs. nontreated retinas; Figs. 6E, 6F). BIX (5 nmol), when co-administered with the tunicamycin, significantly reduced the number of TUNEL-positive cells (vs. tunicamycin alone; Figs. 6F–6H).

Protective Effect of BIX against Tunicamycin-Induced Retinal Damage in Thy-1-CFP Transgenic Mice

In this experiment on Thy-1-CFP transgenic mice, we confirmed the effect of BIX in a larger retinal area than that evaluated in Figure 6D. We counted the number of Thy-1-CFP-positive cells (in flatmounts) in the four white areas shown 1 mm from the center of the optic disc in Figure 7E, and then totaled these values. In the Thy-1-CFP-transgenic mouse retina, axonal fibers were evenly and densely distributed. There were congested CFP-positive cells in the vehicle-treated retina (Fig. 7A), and no change was observed in BIX-treated retinas without tunicamycin treatment (Fig. 7B). Intravitreal injection of tunicamycin decreased the Thy-1-CFP-positive cell count at 7 days (vs. vehicle-treated retina; Figs. 7A, 7C). BIX at 5 nmol, when co-administered with the tunicamycin, significantly inhibited this cell loss (Figs. 7C, 7D, 7F).

Effect of BIX on Tunicamycin-Induced CHOP Expression in Mice

Representative photograph of a nontreated retina is shown in Figure 8A. No change was observed in the BIX-treated retina (Fig. 8B). Optical density analysis of CHOP protein immunoreactivity in GCL and IPL showed that intravitreal injection of tunicamycin (1 μg) significantly increased the level of CHOP protein at 72 h after the injection (Fig. 8C). BIX (5 nmol), when co-administered with the tunicamycin, significantly inhibited this effect (Figs. 8D, 8E).

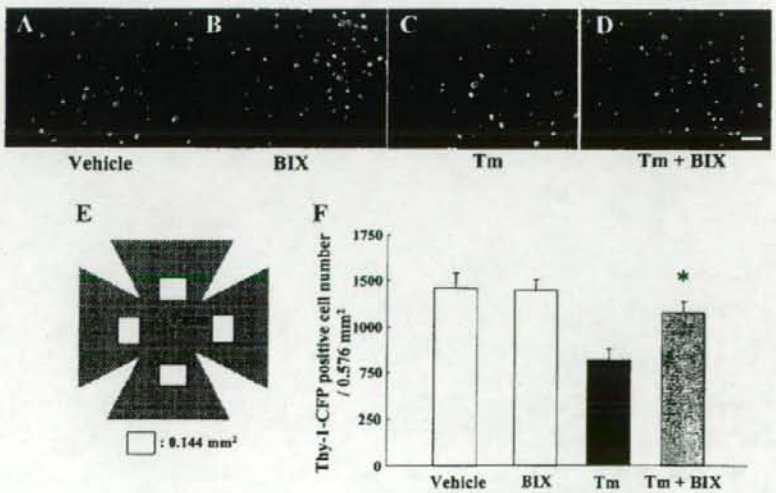

FIGURE 7. Effects of BIX on retinal damage induced by intravitreal injection of tunicamycin in Thy-1-CFP transgenic mice. Mouse retinas (flatmounts) at seven days after intravitreal injection of (A) vehicle, (B) BIX (5 nmol), (C) Tm (1 μg), or (D) Tm (1 μg) plus BIX (5 nmol). Damage was evaluated by counting Thy-1-CFP-positive cell numbers in the four *white* areas shown in (E) (each area 0.144 mm² × 4 areas; total 0.576 mm²) at seven days after the above intravitreal injections. (F) Effect of BIX against Tm-induced damage (indicated by decreased number of Thy-1-CFP-positive cells) at seven days after intravitreal injection. Data are shown as mean ± SE (n = 9 or 10). *$P < 0.05$ versus tunicamycin alone. Scale bar represents 25 μm.

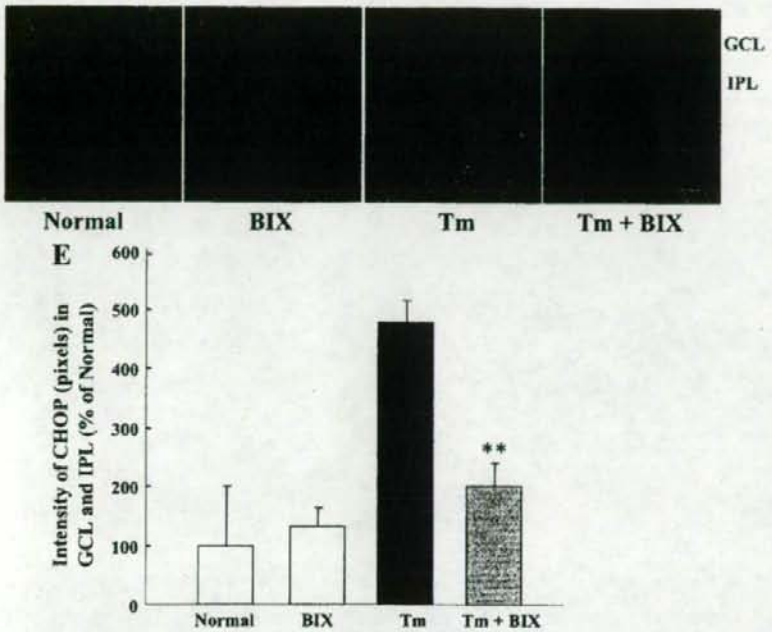

FIGURE 8. Effect of BIX on tunicamycin-induced CHOP expression in the mouse retina. Mouse retinas (cross-sections) either (A) nontreated or at three days after intravitreal injection of (B) BIX (5 nmol), (C) Tm (1 μg) or (D) Tm (1 μg) plus BIX (5 nmol). (E) Relative density of CHOP protein expression in GCL and IPL at three days after the above intravitreal injections. Data are shown as mean ± SE ($n = 6$). $^{**}P < 0.01$ versus tunicamycin alone. Scale bar represents 25 μm.

Effect of BIX on Tunicamycin-Induced XBP-1 Expression in ERAI Mice

In ERAI mice, the fluorescence intensity arising from the XBP-1-venus fusion protein (indicating ER stress activation) can be easily visualized, allowing evaluation of the effect of ER stress on the retina. In the representative photographs of flatmount retinas from ERAI mice shown in Figure 9, no difference was observed between vehicle-treated and BIX-treated retinas (Fig. 9B). Intravitreal injection of tunicamycin (1 μg) induced XBP-1-venus expression (vs. the vehicle-treated retina; Fig. 9C). Immunoblot analysis of XBP-1-venus protein expression in the retina (using an anti-GFP antibody) showed that intravitreal injection of tunicamycin (1 μg) significantly raised the level of XBP-1-venus protein, and that BIX (5 nmol), when co-administered with the tunicamycin (Fig. 9D), significantly inhibited this effect (Figs. 9E, 9F).

Protective Effect of BIX against NMDA-Induced Retinal Damage in Mice

A representative photograph of a nontreated retina is shown in Figure 10A. Intravitreal injection of NMDA (a) decreased the

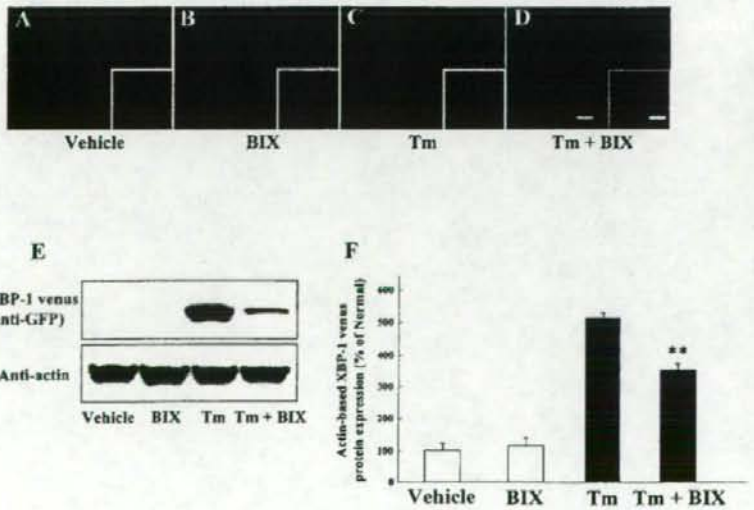

FIGURE 9. Effect of BIX on tunicamycin-induced XBP-1 venus expression in ERAI mice. Mouse retinas (flatmounts) at 24 h after intravitreal injection of (A) vehicle, (B) BIX (5 nmol), (C) Tm (1 μg) or (D) Tm (1 μg) plus BIX (5 nmol). (E) *Upper panel* shows XBP-1 venus protein expression, while *lower panel* shows β-actin protein expression at 24 h after the above injections. (F) Western blot analysis showing effect of BIX on Tm-induced expression of β-actin-based XBP-1 venus protein expression at 24 h after the above injections. Data are shown as mean ± SE ($n = 8$). $^{*}P < 0.01$ versus tunicamycin alone. Scale bars in main photomicrographs and in *insets* represent 25 and 5 μm, respectively.

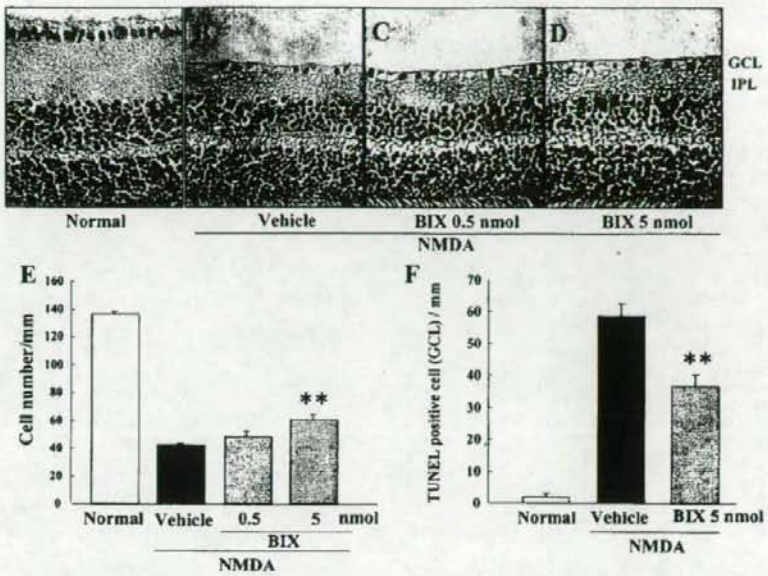

FIGURE 10. Effects of BIX on retinal damage induced by intravitreal injection of NMDA in mice. Mouse retinas (cross-sections) either (A) nontreated or at seven days after intravitreal injection of (B) NMDA (40 nmol) alone or (C, D) NMDA (40 nmol) plus BIX (0.5 or 5 nmol). (E) Damage was evaluated by counting cell numbers in GCL at seven days after the above intravitreal injections. (F) Effect of BIX on NMDA-induced expression of TUNEL-positive cells at 24 h after intravitreal injection of NMDA (40 nmol) either alone or with BIX (5 nmol). Data are shown as mean ± SE ($n = 9$ or 10). $^{**}P < 0.01$ versus NMDA-treated control group. Scale bar represents 25 μm.

cell number in GCL at 7 days (Figs. 10B, 10E) and (b) increased the number of TUNEL-positive cells in GCL at 24 h (vs. nontreated normal retina; Fig. 10F). BIX (5 nmol), when co-administered with the NMDA, significantly reduced (vs. NMDA alone) both the cell loss in GCL (Figs. 10D, 10E) and the number of TUNEL-positive cells (Fig. 10F). On the other hand, there was no statistical difference between BIX (0.5 nmol)- and vehicle-treated group in NMDA-induced cell death in GCL (Figs. 10C, 10E).

Effect of BIX on NMDA-Induced CHOP Expression in Mice

A representative photograph of a nontreated retina is shown in Figure 11A and no change was detected between nontreated

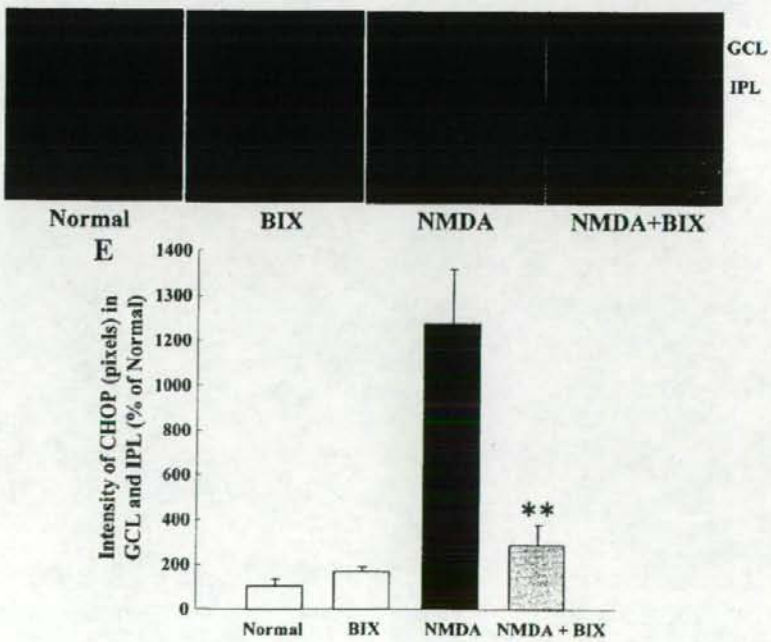

FIGURE 11. Effect of BIX on NMDA-induced CHOP expression in mice. Mouse retinas (cross-sections) either (A) nontreated or at three days after intravitreal injection of (B) NMDA (40 nmol) alone or (C) NMDA (40 nmol), or (D) NMDA (40 nmol) plus BIX (5 nmol). (E) Relative density of CHOP protein expression in GCL and IPL at three days after the above intravitreal injections. Data are shown as mean ± SE ($n = 6$). $^{**}P < 0.01$ versus NMDA alone. Scale bar represents 25 μm.

retina and the BIX-treated retina without NMDA treatment (Figs. 11A, 11B). Optical density analysis of CHOP protein immunoreactivity in GCL and IPL showed that intravitreal injection of NMDA (40 nmol) significantly increased the level of CHOP protein at 72 h after the injection (Fig. 11C). When co-administered with the NMDA, BIX (5 nmol) significantly inhibited this effect (Figs. 11D, 11E).

Discussion

In the present study, we confirmed that BIX preferentially induces BiP mRNA in RGC-5. Although it also induced GRP94, calreticulin, p58^{IPK}, and ASNS, these inductions were lower than that of BiP. This is consistent with our previous study that BIX preferentially induced BiP with slight inductions of GRP94, calreticulin, and CHOP mediated by the activating transcription factor 6 (ATF6) pathway accompanied by activation of ERSEs, and that BIX does not affect the pathway downstream of IRE1 or the translational control branch downstream of PERK in SK-N-SH cells.[32] Therefore, BIX is not just an ER stressor such as tunicamycin or thapsigargin, and we consider that the induction of BiP by BIX is mediated by the ATF6 pathway in RGC-5 similar to that in SK-N-SH cells. Next, we evaluated the effects of BIX, as a preferential inducer of BiP, on ER stress-induced in vitro cell death in RGC-5 (a rat ganglion cell-line) and in vivo retinal damage in mice. We found that BIX reduced tunicamycin-induced cell death in RGC-5 and also reduced both tunicamycin-induced and NMDA-induced retinal damage in mice. Our previous study revealed that BIX (a) reduced tunicamycin-induced cell death in SK-N-SH cells, (b) contributed to the induction of BiP expression via the ATF-6 pathway (but not via the PERK or IRE1 pathways), and (c) on intracerebroventricular injection, prevented the neuronal damage induced by focal ischemia in mice.[32] Furthermore, immunostaining revealed that intravitreal injection of BIX significantly induced BiP protein in mouse retina. Particularly, it expressed in GCL and IPL (versus both the normal and the sham retina). On the other hand, there was little protective effect of BIX against RGC-5 damages after staurosporine treatment. Staurosporine is well known as a nonspecific inhibitor of protein kinases and initiates caspase-dependent apoptosis in many cell types.[41,42] Our previous studies revealed that staurosporine induced cell death without any changes in the expression of BiP or CHOP protein.[12,43] Furthermore, preliminary study showed that treatment with BIX (1 and 5 μM) did not inhibit RGC-5 cell death 48 h after serum deprivation, which does not induce any UPR-responses such as BiP or CHOP (unpublished data). These results strongly support that BIX selectively protects cell damage induced by ER stress.

Recently, we reported that in mice, increased expressions of XBP-1 splicing, BiP, and CHOP could be detected after the induction of retinal damage by tunicamycin, NMDA, or an elevation of intraocular pressure.[13] That report was the first to demonstrate an involvement of ER stress and BiP in retinal cell death in mice. Hence, in the present study we asked whether BIX can prevent such retinal damage. By histologic analysis and TUNEL staining, we estimated that BIX reduced tunicamycin-induced retinal damage in GCL. However, the cell counts in partial cross sections provide a comparatively small sample on which quantitative morphometry can be used to judge such an effect. Therefore, we used Thy-1-CFP transgenic mice[36] to examine the effect of BIX in a large retinal area. This transgene contains a CFP gene under the direction of regulatory elements derived from the mouse Thy-1 gene, and the transgenic mice express CFP protein in RGC and in the inner part of the IPL of the retina.[36] Our results show that BIX exerted a protective effect against tunicamycin-induced retinal damage in the Thy-1-CFP transgenic mouse. However, it is possible that microglial cells become co-labeled with CFP by phagocytosis of the dying RGCs. In this study, we evaluated CFP-positive cells in 7 days after tunicamycin injection. In our previous and preliminary studies, activated microglia cells in GCL were increased at 3 days after NMDA injection[13] and their increases were almost ceased within the 7 days (unpublished data). Furthermore, microglial cells can be distinguished with neuronal cells by their morphologic features.[44] In fact, microglial cells were scarcely observed at seven days after tunicamycin injection, similar to that at seven days after NMDA injection. When we investigated the effect of BIX on NMDA-induced retinal damage in ddY mice, we found that it significantly attenuated such damage. NMDA is well known to induce RGC death and optic-nerve loss (effects mediated by excitatory glutamate receptor), and such neuronal death is believed to play a role in many neurologic and neurodegenerative diseases.[45,46] Recently, Uehara et al.[47] noted that mild exposure to NMDA induced apoptotic cell death in primary cortical culture, and they demonstrated this effect to be caused by an accumulation of polyubiquitinated proteins and increases in XBP-1 mRNA splicing and CHOP mRNA (reflecting activation of the UPR signaling pathway). They also found that protein-disulphide isomerase, which assists in the maturation and transport of unfolded secretory proteins, prevented the neurotoxicity associated with ER stress. These findings suggested that activation of ER stress may participate in the retinal cell death occurring after NMDA-receptor activation and/or an ischemic insult.[47]

In our investigation of the mechanisms underlying the above-mentioned effects, we focused on CHOP. Since CHOP is a member of the CCAAT/enhancer-binding protein family that is induced by ER stress and participates in ER-mediated apoptosis, CHOP may be a key molecule in retinal cell death.[48] We found that treatment with tunicamycin induced apoptotic cell death in RGC-5 and also induced a production of ER stress-related proteins (BiP, the phosphorylated form of eIF2α, and CHOP protein). BIX reduced both the cell death and the CHOP protein expression induced by tunicamycin in RGC-5 in vitro. BIX also attenuated the CHOP protein expression induced by either tunicamycin or NMDA in the mouse retina in vivo. As mentioned above, BIX may affect CHOP protein expression through ATF6 pathway, but no change was observed in BIX-treated RGC-5. In our previous data in SK-N-SH cells, BIX slightly increased CHOP mRNA only at 2 h after the treatment. Expression of CHOP is mainly regulated by three transcription factors—ATF4, cleaved ATF6, and x-box binding protein-1 (XBP-1)—which are downstream effectors during ER stress in similar to other ER chaperones. These differences between BiP and CHOP expression by BIX may be due to the difference of their promoters. CHOP promoter contains at least two ERSE motifs (CHOP ERSE-1 and CHOP ERSE-2) located in opposite directions with a 9 bp overlap, and one of ERSEs is inactive.[49] On the other hand, BiP promoter has three functional ERSE motifs of the rat GRP78 promoter (ERSE-163, ERSE-131, and ERSE-98).[50] These variations in each promoter may contribute to the differences among the expressions of ER chaperons induced by BIX and the lack of CHOP expression.

Subsequently, we monitored XBP-1 activation in the mouse retina in vivo, using ERAI transgenic mice.[37] Effective identification of cells under ER stress conditions is possible in the retina in these mice, as described in our previous report.[13] Here, ERAI mice carrying the F-XBP1ΔDBD–venus expression gene were used to monitor ER stress. The fluorescence intensity arising from the X-box binding protein (XBP1)-venus fusion protein, indicating ER stress activation, was increased in cells within GCL and IPL at 24 h after injection of tunicamycin into the vitreous. BIX significantly reduced this expression, indicating that BIX may attenuate the retinal damage induced

by ER stress-associated factors. In our previous study,[32] we found that BIX induced BiP protein expression via the ATF-6 pathway (not via other ER stress-associated factors such as the PERK and IRE1 pathways) in SK-N-SH cells. Possibly, the protective mechanism underlying the effect of BIX on the mouse retina may be the same as that revealed by our previous study, but further experiments will be needed to clarify this issue.

In conclusion, we have demonstrated that BIX, a preferential inducer of BiP, inhibits both the neuronal cell death induced by ER stress in vitro in RGC-5 cells and in vivo in the mouse retina. Hence, an increase in BiP might be one of the targets of mechanisms bestowing neuroprotection in retinal diseases.

Acknowledgments

The authors thank Masayuki Miura (Department of Genetics, Graduate School of Pharmaceutical Sciences, University of Tokyo, Tokyo, Japan) for the kind gift of ERAI mice, and Rumi Uchibayashi and Shunsake Imai for technical assistance.

References

1. Travers KJ, Patil CK, Wodicka L, Lockhart DJ, Weissman JS, Walter P. Functional and genomic analyses reveal an essential coordination between the unfolded protein response and ER-associated degradation. *Cell.* 2000;101:249–258.
2. Harding HP, Novoa I, Zhang Y, et al. Regulated translation initiation controls stress-induced gene expression in mammalian cells. *Mol Cell.* 2000;6:1099–1108.
3. Schroder M, Kaufman RJ. The mammalian unfolded protein response. *Annu Rev Biochem.* 2005;74:739–789.
4. Katayama T, Imaizumi K, Honda A, et al. Disturbed activation of endoplasmic reticulum stress transducers by familial Alzheimer's disease-linked presenilin-1 mutations. *J Biol Chem.* 2001;276:43446–43454.
5. Ryu EJ, Harding HP, Angelastro JM, Vitolo OV, Ron D, Greene LA. Endoplasmic reticulum stress and the unfolded protein response in cellular models of Parkinson's disease. *J Neurosci.* 2002;22:10690–10698.
6. Oyadomari S, Koizumi A, Takeda K, et al. Targeted disruption of the Chop gene delays endoplasmic reticulum stress-mediated diabetes. *J Clin Invest.* 2002;109:525–532.
7. Roybal CN, Yang S, Sun CW, et al. Homocysteine increases the expression of vascular endothelial growth factor by a mechanism involving endoplasmic reticulum stress and transcription factor ATF4. *J Biol Chem.* 2004;279:14844–14852.
8. Rebello G, Ramesar R, Vorster A, et al. Apoptosis-inducing signal sequence mutation in carbonic anhydrase IV identified in patients with the RP17 form of retinitis pigmentosa. *Proc Natl Acad Sci USA.* 2004;101:6617–6622.
9. Lin JH, Li H, Yasumura D, et al. IRE1 signaling affects cell fate during the unfolded protein response. *Science.* 2007;318:944–949.
10. Joe MK, Sohn S, Hur W, Moon Y, Choi YR, Kee C. Accumulation of mutant myocilins in ER leads to ER stress and potential cytotoxicity in human trabecular meshwork cells. *Biochem Biophys Res Commun.* 2003;312:592–600.
11. Gould DB, Marchant JK, Savinova OV, Smith RS, John SW. Col4a1 mutation causes endoplasmic reticulum stress and genetically modifiable ocular dysgenesis. *Hum Mol Genet.* 2007;16:798–807.
12. Shimazawa M, Ito Y, Inokuchi Y, Hara H. Involvement of double-stranded RNA-dependent protein kinase in ER stress-induced retinal neuron damage. *Invest Ophthalmol Vis Sci.* 2007;48:3729–3736.
13. Shimazawa M, Inokuchi Y, Ito Y, et al. Involvement of ER stress in retinal cell death. *Mol Vis.* 2007;13:578–587.
14. Mahoney WC, Duksin D. Biological activities of the two major components of tunicamycin. *J Biol Chem.* 1979;254:6572–6576.
15. Awai M, Koga T, Inomata Y, et al. NMDA-induced retinal injury is mediated by an endoplasmic reticulum stress-related protein, CHOP/GADD153. *J Neurochem.* 2006;96:43–52.
16. Lee YK, Brewer JW, Hellman R, Hendershot LM. BiP and immunoglobulin light chain cooperate to control the folding of heavy chain and ensure the fidelity of immunoglobulin assembly. *Mol Biol Cell.* 1999;10:2209–2219.
17. Li WW, Alexandre S, Cao X, Lee AS. Transactivation of the grp78 promoter by Ca^{2+} depletion. A comparative analysis with A23187 and the endoplasmic reticulum Ca^{2+}-ATPase inhibitor thapsigargin. *J Biol Chem.* 1993;268:12003–12009.
18. van de Put FH, Elliott AC. The endoplasmic reticulum can act as a functional Ca^{2+} store in all subcellular regions of the pancreatic acinar cell. *J Biol Chem.* 1997;272:27764–27770.
19. Lievremont JP, Rizzuto R, Hendershot L, Meldolesi J. BiP, a major chaperone protein of the endoplasmic reticulum lumen, plays a direct and important role in the storage of the rapidly exchanging pool of Ca^{2+}. *J Biol Chem.* 1997;272:30873–30879.
20. Helenius A. How N-linked oligosaccharides affect glycoprotein folding in the endoplasmic reticulum. *Mol Biol Cell.* 1994;5:253–265.
21. Kuznetsov G, Chen LB, Nigam SK. Multiple molecular chaperones complex with misfolded large oligomeric glycoproteins in the endoplasmic reticulum. *J Biol Chem.* 1997;272:3057–3063.
22. Klausner RD, Sitia R. Protein degradation in the endoplasmic reticulum. *Cell.* 1990;62:611–614.
23. Blond-Elguindi S, Cwirla SE, Dower WJ, et al. Affinity panning of a library of peptides displayed on bacteriophages reveals the binding specificity of BiP. *Cell.* 1993;75:717–728.
24. Knarr G, Gething MJ, Modrow S, Buchner J. BiP binding sequences in antibodies. *J Biol Chem.* 1995;270:27589–27594.
25. Knarr G, Modrow S, Todd A, Gething MJ, Buchner J. BiP-binding sequences in HIV gp160. Implications for the binding specificity of bip. *J Biol Chem.* 1999;274:29850–29857.
26. Brodsky JL, Werner ED, Dubas ME, Goeckeler JL, Kruse KB, McCracken AA. The requirement for molecular chaperones during endoplasmic reticulum-associated protein degradation demonstrates that protein export and import are mechanistically distinct. *J Biol Chem.* 1999;274:3453–3460.
27. Meerovitch K, Wing S, Goltzman D. Proparathyroid hormone-related protein is associated with the chaperone protein BiP and undergoes proteasome-mediated degradation. *J Biol Chem.* 1998;273:21025–21030.
28. Katayama T, Imaizumi K, Sato N, et al. Presenilin-1 mutations downregulate the signalling pathway of the unfolded-protein response. *Nat Cell Biol.* 1999;1:479–485.
29. Yu Z, Luo H, Fu W, Mattson MP. The endoplasmic reticulum stress-responsive protein GRP78 protects neurons against excitotoxicity and apoptosis: suppression of oxidative stress and stabilization of calcium homeostasis. *Exp Neurol.* 1999;155:302–314.
30. Rao RV, Peel A, Logvinova A, et al. Coupling endoplasmic reticulum stress to the cell death program: role of the ER chaperone GRP78. *FEBS Lett.* 2002;514:122–128.
31. Reddy RK, Mao C, Baumeister P, Austin RC, Kaufman RJ, Lee AS. Endoplasmic reticulum chaperone protein GRP78 protects cells from apoptosis induced by topoisomerase inhibitors: role of ATP binding site in suppression of caspase-7 activation. *J Biol Chem.* 2003;278:20915–20924.
32. Kudo T, Kanemoto S, Hara H, et al. A molecular chaperone inducer protects neurons from ER stress. *Cell Death Differ.* 2008;15:364–375.
33. Krishnamoorthy RR, Agarwal P, Prasanna G, et al. Characterization of a transformed rat retinal ganglion cell line. *Brain Res Mol Brain Res.* 2001;86:1–12.
34. Chen D, Padiernos E, Ding F, Lossos IS, Lopez CD. Apoptosis-stimulating protein of p53-2 (ASPP2/53BP2L) is an E2F target gene. *Cell Death Differ.* 2005;12:358–368.
35. Jiang Y, Ahn EY, Ryu SH, et al. Cytotoxicity of psammaplin A from a two-sponge association may correlate with the inhibition of DNA replication. *BMC Cancer.* 2004;4:70.
36. Feng G, Mellor RH, Bernstein M, et al. Imaging neuronal subsets in transgenic mice expressing multiple spectral variants of GFP. *Neuron.* 2000;28:41–51.
37. Iwawaki T, Akai R, Kohno K, Miura M. A transgenic mouse model for monitoring endoplasmic reticulum stress. *Nat Med.* 2004;10:98–102.

38. Siliprandi R, Canella R, Carmignoto G, et al. N-methyl-D-aspartate-induced neurotoxicity in the adult rat retina. *Vis Neurosci.* 1992; 8:567–573.
39. Jeon CJ, Strettoi E, Masland RH. The major cell populations of the mouse retina. *J Neurosci.* 1998;18:8936–8946.
40. Onozuka T, Sawamura D, Goto M, Yokota K, Shimizu H. Possible role of endoplasmic reticulum stress in the pathogenesis of Darier's disease. *J Dermatol Sci.* 2006;41:217–220.
41. Weil M, Jacobson MD, Coles HS, et al. Constitutive expression of the machinery for programmed cell death. *J Cell Biol.* 1996;133: 1053–1059.
42. Taylor J, Gatchalian CL, Keen G, Rubin LL. Apoptosis in cerebellar granule neurones: involvement of interleukin-1 beta converting enzyme-like proteases. *J Neurochem.* 1997;68:1598–1605.
43. Inokuchi Y, Shimazawa M, Nakajima Y, Suemori S, Mishima S, Hara H. Brazilian green propolis protects against retinal damage in vitro and in vivo. *Evid Based Complement Alternat Med.* 2006;3:71–77.
44. Chidlow G, Wood JP, Manavis J, Osborne NN, Casson RJ. Expression of osteopontin in the rat retina: effects of excitotoxic and ischemic injuries. *Invest Ophthalmol Vis Sci.* 2008;49:762–771.
45. Sucher NJ, Lipton SA, Dreyer EB. Molecular basis of glutamate toxicity in retinal ganglion cells. *Vision Res.* 1997;37:3483–3493.
46. Henneberry RC, Novelli A, Cox JA, Lysko PG. Neurotoxicity at the N-methyl-D-aspartate receptor in energy-compromised neurons. An hypothesis for cell death in aging and disease. *Ann NY Acad Sci.* 1989;568:225–233.
47. Uehara T, Nakamura T, Yao D, et al. S-nitrosylated protein-disulphide isomerase links protein misfolding to neurodegeneration. *Nature.* 2006;441:513–517.
48. Wang XZ, Lawson B, Brewer JW, et al. Signals from the stressed endoplasmic reticulum induce C/EBP-homologous protein (CHOP/GADD153). *Mol Cell Biol.* 1996;16:4273–4280.
49. Ubeda M, Habener JF. CHOP gene expression in response to endoplasmic-reticular stress requires NFY interaction with different domains of a conserved DNA-binding element. *Nucleic Acids Res.* 2000;28:4987–4997.
50. Foti DM, Welihinda A, Kaufman RJ, Lee AS. Conservation and divergence of the yeast and mammalian unfolded protein response. Activation of specific mammalian endoplasmic reticulum stress element of the grp78/BiP promoter by yeast Hac1. *J Biol Chem.* 1999;274:30402–30409.

Current Eye Research, 33:247–252, 2008

ISSN: 0271-3683 print / 1460-2202 online
DOI: 10.1080/02713680801919716

informa
healthcare

The Efficacy of TonoLab in Detecting Physiological and Pharmacological Changes of Mouse Intraocular Pressure–Comparison with TonoPen and Microneedle Manometery

Tadashiro Saeki, Makoto Aihara, Masaaki Ohashi, and Makoto Araie
Department of Ophthalmology, University of Tokyo School of Medicine, Tokyo, Japan

ABSTRACT *Purpose*: The efficacy of two non-invasive tonometers, TonoLab and TonoPen XL, in detecting physiological or pharmacological changes of intraocular pressure (IOP) in mouse eyes, was assessed by comparison with a microneedle method. *Material and Methods:* C57BL6 mice, bred under the 12-hr light and dark cycle over 2 weeks, were used. Under systemic anesthesia, mouse eyes were cannulated by a microneedle connected to a transducer and a water reservoir. We manipulated the intracameral pressure by changing the reservoir height, and obtained tonometer readings at each pressure ($n = 39$) with TonoLab and TonoPen XL. The correlation between each tonometer and the manometer was analyzed. Then the diurnal variation of IOP in the light and dark phases, and the IOP-lowering effect at 2 hr after latanoprost instillation, were measured with TonoLab, TonoPen XL, and a microneedle tonometer ($n = 8$). *Results:* In mouse eyes, TonoPen XL could not show reliable scores, but TonoLab readings showed a strong correlation with manometer readings ($y = 0.87x - 0.27$, $r^2 = 0.917$). Nocturnal elevation of IOP in mouse eyes was significantly indicated with TonoLab and a microneedle tonometer ($p < 0.001$), but not with TonoPen XL. Latanoprost significantly reduced IOP by 2.1 ± 2.8 and 2.0 ± 1.0 mmHg with TonoLab and a microneedle tonometer, but not with TonoPen XL. *Conclusion:* TonoLab provides similar readings to a microneedle tonometer, and diurnal variation and drug effect were detectable in mouse eyes. TonoLab promises to be a non-invasive and useful method to evaluate physiological and pharmacological studies in mouse eyes.

KEYWORDS diurnal variation; intraocular pressure; latanoprost; mouse; tonometer

Received 16 November 2007
Accepted 15 January 2008

Correspondence: Makoto Aihara, M.D., Ph.D., Department of Ophthalmology, University of Tokyo School of Medicine, 7-3-1 Hongo, Bunkyo-ku Tokyo 113-8655, Japan. E-mail: aihara-tky@umin.ac.jp

INTRODUCTION

Mouse models are well established in mimicking glaucoma and other conditions with high intraocular pressure (IOP) and in evaluating the IOP-lowering mechanism of drugs. They are easily bred at relatively low cost in a controlled

environment and are also amenable to genetic manipulation. To expand the possibility of using mouse eyes for glaucoma research, accurate and reproducible IOP measurement is indispensable. However, it is difficult to measure IOP in mice because of their small size. A direct measurement, using a microneedle cannulation into the anterior chamber connected to a transducer, can record intracameral pressure directly and with accuracy,[1–3] but this procedure is invasive, so it cannot be used at short intervals, and it carries a risk of infection or inflammation.

In recent years, some noninvasive and repeatable methods of measuring IOP in mice have been reported.[4–6] The TonoPen XL® electronic tonometer (TonoPen, Mentor, Santa Barbara, CA, USA) was the most popular noninvasive method.[5,7] There were many reports of IOP measurement in rat eyes using TonoPen, even in conscious rats, but it was originally designed for use in humans,[8] and it may be surmised that it will be less accurate in these small animals.[9] Special care was needed to avoid pushing the eyes in measurement, because it causes overestimation of the IOP.

Recently, the TonoLab® rebound tonometer (TonoLab, Tiolat, Helsinki, Finland) has become commercially available; it was the first tonometer designed for use in mice.[9] This instrument is small (handheld) and suitable for repeated use, and its lightweight probe makes it possible to make measurements with less artificial pressure. TonoLab readings are well related to manometric intracameral pressure.[7,10,11] Moreover, TonoLab has been found to be a valuable tool to evaluate mouse IOP, including the glaucoma model mouse DBA2J.[7] It is also more accurate than TonoPen.[10]

In mouse glaucoma models with high IOP, therefore, TonoLab may be more useful than TonoPen. However, mouse eyes, which show great promise in basic glaucoma research, require highly accurate IOP measurements to expand their usage possibilities. Thus far, the potential of these non-invasive tonometers in detecting physiological and pharmacological change of IOP has not been assessed.

In this study, TonoLab and TonoPen were used to measure IOP in mouse eyes in comparison with a microneedle manometer. Subsequently, the diurnal rhythm of intraocular pressure and the effect of topical latanoprost were assessed and compared among these instruments.

MATERIALS AND METHODS

Animals

Male C57BL6 mice (8 weeks old) were obtained from Saitama Jikken Dobutsu (Saitama, Japan). All mice were housed in clear plastic cages covered loosely with air filters and containing white pine shavings for bedding. All studies were in compliance with the Association for Research in Vision and Ophthalmology (ARVO) Resolution on the Use of Animals in Research, and also approved by local ethical committee for animal studies. The animals were entrained to a light schedule of alternating 12-hr periods of light and dark (12 L, 12 D, light on at 6:00 AM), with free access to food and water.

IOP Measurement

The mice were anesthetized by intraperitoneal injection of a mixture of ketamine (100 mg/kg) and xylazine (9 mg/kg), prepared at room temperature. Then topical 0.4% oxybuprocaine (Benoxyl®; Santen Pharmaceuticals, Osaka, Japan) was applied in both eyes before each experiment.

We used three instruments to measure IOP; the microneedle method, TonoPen, and TonoLab. Intraocular pressure was measured directly by the microneedle method in anesthetized mice as previously described.[1] Briefly, after loss of consciousness, the animal was placed in a restrainer that maintained a prone body position similar to awake mice and gently immobilized the head. The microneedle was connected to a pressure transducer, which relayed its signal to a bridge amplifier, and hence to an analogue-to-digital converter and computer. The microneedle tip was inserted through the cornea, and the data were automatically collected online into a computer database. To minimize variation in our measurements due to stress or physical activity, the IOP was measured under anesthesia. In addition, data were collected during a time window 4–6 min after injection of anesthetic during which IOP has been shown to plateau.[1]

With the TonoPen, values ranging from 6 mmHg to 69 mmHg were recorded without automatically averaged readings; we averaged 15 valid readings for one measurement. With the TonoLab, automatically averaged readings were recorded. When the statistical reliability of the average measurement, as represented by

the coefficient of variance of the measurement, was not minimal, the reading in both measurements with TonoPen and TonoLab was ignored and another measurement taken.

Manometric Calibration of the TonoPen and TonoLab

A glass microneedle (for mouse eyes) was inserted into the anterior chamber at the limbus of the right eye under a stereoscopic microscope, taking care to avoid lens injury. The absence of leakage around the needle was confirmed and corneal deformation was minimized by monitoring the intracameral pressure variation, as described below. The needle was connected to a three-way connector, which in turn was connected in parallel to a pressure transducer and a fluid reservoir (BSS Plus®; Alcon Laboratories, Fort Worth, TX, USA). The intracameral pressure could be increased or decreased by moving a fluid reservoir up or down while monitoring actual intracameral pressure with the pressure transducer. Calibration was performed using 8 eyes. In one eye, one pressure setting was performed every 5 mmHg between 5 mmHg and 30 mmHg. Thus, 5 pressures were set in one eye of 8 mice, in total 40 measurement settings.

The measurement of IOP with TonoPen or TonoLab was performed blind to the position of the reservoir and the transducer readings. Each measurement was plotted against the corresponding manometric values. Linear regression analyses were performed to obtain a mathematical formulation of the relationship between tonometric measurements and the manometric values.

Timeframe and the Order of Three Methods for IOP Measurements

IOP was measured using 8 mice for each method. Considering the pressure lowering by repeated IOP measurements, on the first day of experiments IOP was measured by TonoLab, and continuously measured by TonoPen with 30-min intervals. On the second day, IOP was measured by a microneedle method in the same timeframe. Considering the diurnal variation of IOP, all IOP measurements were finished within 1 hr in each day.

Diurnal Variation of IOP in Normal Mouse

IOP at 09:00 and 21:00 was measured in 8 mice with TonoLab, TonoPen, and the microneedle method. With TonoLab and TonoPen, IOP was measured in the same day in the same eyes, but with the microneedle, and one week's interval was allowed between the measurement at both times because of its penetration into the eye.

Effect of Topical Instillation of Latanoprost on Mouse IOP

We evaluated the effect of topical latanoprost (Xalatan; Pharmacia, Uppsala, Sweden) in 8 mouse eyes, using the three instruments, TonoLab, TonoPen, and the microneedle tonometer. At 16:00, latanoprost (0.005%, and 3 μl for mouse) was instilled into one randomly selected eye of each animal, and carrier solution was administered topically to the other eye as a control. General anesthesia was administered at 17:45. Two hours after instillation (18:00), IOP was measured in a masked manner. The ocular hypotensive effect was evaluated by comparison of the IOP between treated and untreated (contralateral) eyes.

Statistics

All data are shown as mean ± standard deviation. The difference between IOP measured at daytime and nighttime, and the difference between eyes treated with or without latanoprost, were statistically evaluated by means of a paired t-test.

RESULTS

TonoLab and TonoPen Measurement in Mouse Eyes (Fig. 1)

As shown in Figure 1B, the tip of the TonoPen was so large that, in the mouse, eye distortion and indentation of the globe or attachment of the tip to the eyelashes or lid were inevitable. In this study, a reliable score from TonoPen was not obtained in mouse eyes. Thus, only TonoLab was compared to the microneedle method.

Manometric Calibration of the TonoLab in Mouse Eyes (Fig. 2)

Calibration was performed at 5 pressure values per eye using 8 eyes. In practice, pressure settings were not

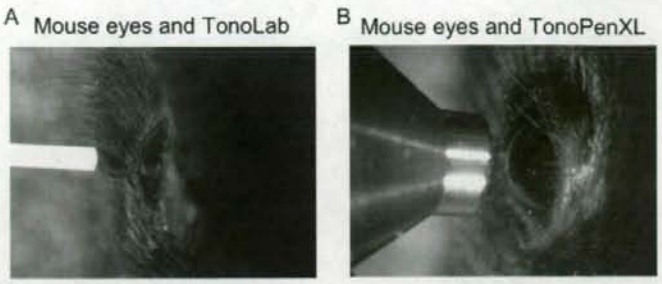

FIGURE 1 TonoLab and TonoPen measurement in mouse eyes. (A) The tip of TonoLab against mouse eyes. (B) The tip of TonoPen against mouse eyes. Note the diameter of both tips for eyeballs.

exact 5-mmHg intervals, as shown in Figure 2, and one measurement was failed. Thus, the total number became 39. A regression line was calculated by plotting TonoLab readings (39 different intracameral pressures) against the corresponding manometric values, and the formula, $y = 0.87x - 0.27$ was determined, where x represents the pressure measured with the pressure transducer and y represents the mean TonoLab readings. The correlation coefficient for TonoLab was $r^2 = 0.917$ (Fig. 2).

Diurnal Variation of IOP in Mouse (Fig. 3)

The mean IOP of the light phase was measured as 8.1 ± 0.6 and 9.8 ± 0.4 mmHg with TonoLab and the microneedle method, respectively ($n = 8$), with the mean IOP of the dark phase measuring 15.4 ± 2.1 and 18.4 ± 0.7 mmHg. There were significant IOP differences between the light- and dark-phase IOPs measured with TonoLab (8.1 ± 0.6 vs. 15.4 ± 2.1, $p = 0.012$ by paired t-test), and the microneedle method (9.8 ± 0.4 vs. 18.4 ± 0.7, $p < 0.001$ by paired t-test).

Effect of Topical Instillation of Latanoprost on Mouse IOP (Fig. 4)

Using TonoLab, the IOPs treated by carrier solution and latanoprost were measured as 12.5 ± 1.8 and 10.4 ± 2.0 mmHg ($p = 0.040$, paired t-test), respectively, and by the microneedle method as 14.4 ± 1.1 and 12.4 ± 1.4 mmHg ($p < 0.001$, paired t-test) ($n = 8$). The mean reductions in IOP shown by the two methods were 2.1 ± 2.8 and 2.0 ± 1.0 mmHg, respectively,

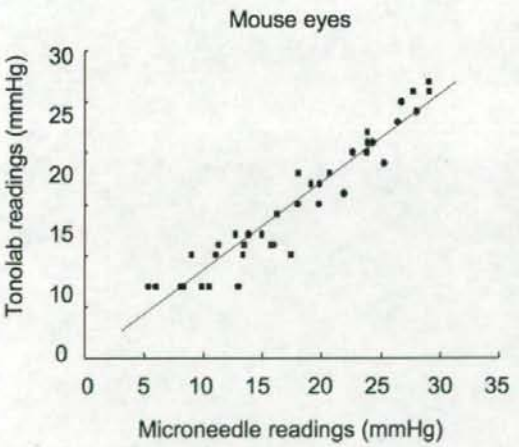

FIGURE 2 Calibration of the TonoLab and TonoPen XL in mouse eyes. Scatter diagram for TonoLab ($n = 39$) readings against the corresponding manometric values in mouse eyes. Regression line formula is $y = 0.87x - 0.27$ ($r^2 = 0.917$) for TonoLab.

FIGURE 3 Circadian rhythm of IOP in normal mouse. IOP are measured at 9:00 AM and 9:00 PM with TonoLab (white column) and a microneedle (black column) in mouse eyes ($n = 8$). The data are the mean ± SD. * $p < 0.001$, by paired t-test.

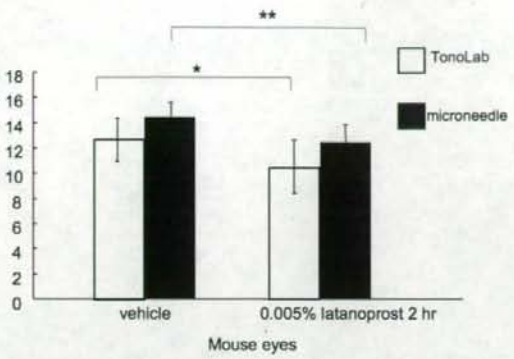

FIGURE 4 Effect of topical instillation of latanoprost on mouse IOP. IOP in both eyes was measured 2 hr after administration of latanoprost or vehicle with TonoLab (white column), and a microneedle (black column) in mouse eyes. The data are the mean ± SD. Asterisks indicate significance by paired *t*-test. $^{*}p = 0.040$, $^{**}p < 0.001$.

and, with both, latanoprost significantly reduced IOP in mouse eyes ($p < 0.001$) (Fig. 4).

DISCUSSION

Recently, many rodent glaucoma models have been developed and characterized, but accurate IOP measurement with non-invasive instrumentation remained one of the most challenging tasks in such experiments. The TonoPen is widely used for rats and also used for mice among some investigators, but it requires a lot of training and experience for accurate and reproducible measurement in rat eyes, still more in mouse eyes. In our study, we were unable to obtain reliable scores in mouse eyes and finally abandoned the use of TonoPen for them. To date, TonoPen has been used in a few studies to measure high IOP in mouse glaucoma models such as DBA2J or other artificially modified mice,[12,13] but, recently, TonoLab has been used more in these glaucoma model mice.[7,14] This tendency underlines the difficulty in measuring rodent IOPs with TonoPen.

The tip of TonoPen is hard, and the tonometer itself is in direct contact with the eye. The effect of impact on the eye is thought incompatible with accurate measurements in glaucoma mouse models. As shown in Figure 1, the tip of the TonoPen is quite large against the mouse globe. Thus, with the globe in its natural position, a clean contact without pushing the eyeballs or contacting the eyelashes and lids was impossible to achieve. In contrast, the ultra-lightweight probe of the TonoLab needs to be ejected magnetically from the instrument only a few times to obtain a viable reading. The impact appears minimal compared with that of other instruments. In addition, it is possible to become proficient in this method without special training.

In this study, we compared the accuracy of TonoLab tonometers and a microneedle method in mice to assess their potential to detect the slight change of IOP in physiological diurnal variation or through treatment with ocular hypertensive agents. We found that TonoLab can detect these changes well in mouse eyes with some benefits. Of course, non-invasive measurement has some drawbacks, notably the lower accuracy of the IOP value compared to that measured by a microneedle.

IOP measurement with TonoLab, which can detect the diurnal changes, has a potential to clarify the molecular mechanisms of diurnal changes of IOP using normal or various kinds of transgenic mouse eyes. Already, diurnal variation of mouse IOP were different among the strains,[15] varied by light conditions,[16,17] and modified by a clock gene.[18] In these studies, diurnal variation of mouse IOP was measured by a microneedle method because TonoLab was not developed, although TonoPen had been already present. Our result suggests the potential use of TonoLab for future studies, additionally, considering diurnal changes are important to development of ocular hypotensive drugs, or to clarify the mechanism of IOP reduction. For example, IOP-lowering effect by prostaglandin analogues was obviously higher in the nighttime than that in the daytime.[19] Thus, drug screening considering diurnal variation of IOP is more effective and important in mouse eyes. Moreover, non-invasive measurement of IOP with TonoLab is repeatable in the same eye with a short interval compared to the invasive microneedle method, which leads to reduce the number of experimental animals.

Moreover, repeated measurement in the same eye permits easy detection of the effect of drugs such as beta-blockers affecting the IOP in the contralateral eye through systemic circulation following absorption through the mucosal tissue. This cannot be evaluated by an invasive microneedle method. Also, TonoLab can be used in the awake mice. Thus, IOP may be evaluated in more physiological conditions compared to that under anesthesia.

Taken together, TonoLab is a significant advance and convenient instrument for use in small animal

eyes. Therefore, our study to indicate the usefulness of TonoLab for the measurement of physiological or pharmacological changes in mouse IOP may be worth expanding the application of mouse eyes for glaucoma studies.

ACKNOWLEDGMENTS

Supported in part by grants H18-Kankakuippan-001 from the Ministry of Health, Labor, and Welfare of Japan, and A18209053 from the Ministry of Education, Culture, Sports, Science, and Technology of Japan.

REFERENCES

[1] Aihara M, Lindsey JD, Weinreb RN. Reduction of intraocular pressure in mouse eyes treated with latanoprost. *Invest Ophthalmol Vis Sci*. 2002;43:146–150.

[2] Avila MY, Carre DA, Stone RA, Civan MM. Reliable measurement of mouse intraocular pressure by a servo-null micropipette system. *Invest Ophthalmol Vis Sci*. 2001;42:1841–1846.

[3] John SW, Hagaman JR, MacTaggart TE, Peng L, Smithes O. Intraocular pressure in inbred mouse strains. *Invest Ophthalmol Vis Sci*. 1997;38:249–253.

[4] Cohan BE, Bohr DF. Measurement of intraocular pressure in awake mice. *Invest Ophthalmol Vis Sci*. 2001;42:2560–2562.

[5] Reitsamer HA, Kiel JW, Harrison JM, Ransom NL, McKinnon SJ. TonoPen measurement of intraocular pressure in mice. *Exp Eye Res*. 2004;78:799–804.

[6] Filippopoulos T, Matsubara A, Danias J, Huang W, Dobberfuhl A, Ren L, Mittag T, Miller JW, Grosskreutz CL. Predictability and limitations of non-invasive murine tonometry: Comparison of two devices. *Exp Eye Res*. 2006;83:194–201.

[7] Wang WH, Millar JC, Pang IH, Wax MB, Clark AF. Noninvasive measurement of rodent intraocular pressure with a rebound tonometer. *Invest Ophthalmol Vis Sci*. 2005;46:4617–4621.

[8] Midelfart A, Wigers A. Clinical comparison of the ProTon and TonoPen tonometers with the Goldmann applanation tonometer. *Br J Ophthalmol*. 1994;78:895–898.

[9] Dalke C, Pleyer U, Graw J. On the use of TonoPen XL for the measurement of intraocular pressure in mice. *Exp Eye Res*. 2005;80:295–296.

[10] Pease ME, Hammond JC, Quigley HA. Manometric calibration and comparison of TonoLab and TonoPen tonometers in rats with experimental glaucoma and in normal mice. *J Glaucoma*. 2006;15:512–519.

[11] Morris CA, Crowston JG, Lindsey JD, Danias J, Weinreb RN. Comparison of invasive and non-invasive tonometry in the mouse. *Exp Eye Res*. 2006;82:1094–1099.

[12] Gross RL, Ji J, Chang P, Pennesi ME, Yang Z, Zhang J, Wu SM. A mouse model of elevated intraocular pressure: Retina and optic nerve findings. *Trans Am Ophthalmol Soc*. 2003;101:163–169; discussion 169–171.

[13] Ueda J, Sawaguchi S, Hanyu T, Yaoeda K, Fukuchi T, Abe H, Ozawa H. Experimental glaucoma model in the rat induced by laser trabecular photocoagulation after an intracameral injection of India ink. *Jpn J Ophthalmol*. 1998;42:337–344.

[14] Danias J, Lee KC, Zamora MF, Chen B, Shen F, Filippopoulos T, Su Y, Goldblum D, Podos SM, Mittag T. Quantitative analysis of retinal ganglion cell (RGC) loss in aging DBA/2NNia glaucomatous mice: Comparison with RGC loss in aging C57/BL6 mice. *Invest Ophthalmol Vis Sci*. 2003;44:5151–5162.

[15] Savinova OV, Sugiyama F, Martin JE, Tomarev SI, Paigen BJ, Smith RS, John SW. Intraocular pressure in genetically distinct mice: An update and strain survey. *BMC Genet*. 2001;2:12.

[16] Aihara M, Lindsey JD, Weinreb RN. Twenty-four-hour pattern of mouse intraocular pressure. *Exp Eye Res*. 2003;77:681–686.

[17] Sugimoto E, Aihara M, Ota T, Araie M. Effect of light cycle on 24-hour pattern of mouse intraocular pressure. *J Glaucoma*. 2006;15:505–511.

[18] Maeda A, Tsujiya S, Higashide T, Toida K, Todo T, Ueyama T, Okamura H, Sugiyama K. Circadian intraocular pressure rhythm is generated by clock genes. *Invest Ophthalmol Vis Sci*. 2006;47:4050–4052.

[19] Ota T, Murata H, Sugimoto E, Aihara M, Araie M. Prostaglandin analogues and mouse intraocular pressure: Effects of tafluprost, latanoprost, travoprost, and unoprostone, considering 24-hour variation. *Invest Ophthalmol Vis Sci*. 2005;46:2006–2011.

Imaging Mouse Retinal Ganglion Cells and Their Loss In Vivo by a Fundus Camera in the Normal and Ischemia-Reperfusion Model

Hiroshi Murata,[1] Makoto Aihara,[2] Yi-Ning Chen,[2] Takashi Ota,[2] Jiro Numaga,[1] and Makoto Araie[2]

Purpose. To visualize retinal ganglion cells (RGCs) and their gradual loss in the living mouse.

Methods. With the use of B6.Cg-Tg(Thy1-CFP)23Jrs/J mice, which express cyan fluorescent protein (CFP) in RGCs, and a commercially available mydriatic retinal camera attached with a 5 million-pixel digital camera to visualize RGCs in vivo, the authors recorded fundus photographs longitudinally in the ischemia reperfusion model group and the untreated group to evaluate longitudinal changes in the number of RGCs in experimental models. Moreover, RGCs expressing CFP were evaluated histologically by a retrograde-labeling method and retinal whole mount or sections.

Results. The authors devised an in vivo imaging technique using a conventional retinal camera and visualized RGCs at the single-cell level. In the ischemia reperfusion model, a longitudinal reduction in the number of RGCs was demonstrated in each mouse eye. The number of RGCs and the fluorescence intensity of the nerve fiber decreased considerably during the first week. The percentages of RGCs decreased to 34.2% ± 7.5%, 24.1% ± 9.1%, 23.0% ± 9.3%, and 22.2% ± 8.4% (mean ± SD, $n = 5$) of the percentages before injury at 1, 2, 3, and 4 weeks after injury, respectively ($P < 0.001$). In this transgenic mouse, 97% of CFP-expressing cells were RGCs and 73% of RGCs expressed CFP.

Conclusions. This in vivo technique allows noninvasive, repeated, and longitudinal evaluation of RGCs for investigation of retinal neurodegenerative diseases and new therapeutic modalities for them. (*Invest Ophthalmol Vis Sci.* 2008;49:5546–5552) DOI:10.1167/iovs.07-1211

The neural retina and the optic disc are the only neuronal tissues that can be visualized in vivo without any invasive manipulation, and a great improvement has recently been achieved in imaging techniques for the evaluation of the human retina and optic nerve head (ONH).[1,2] Glaucoma, the second leading cause of vision loss in the world,[3] is associated with damage of optic nerve axons at the ONH and their cell bodies, the retinal ganglion cells (RGCs).[4] The only therapy available to stem RGC death in glaucoma is the reduction of intraocular pressure (IOP),[5] which is especially effective in patients with elevated IOP. However, elevated IOP is not the only pathogenic factor of glaucoma.[6]

Experimental neurodegenerative models such as ischemia reperfusion, optic nerve crush, intravitreal glutamate injection, and experimental ocular hypertension[7] have been used to investigate the pathogenesis of RGC death and possible neuroprotective treatment against it, for which reliable evaluation of the number of living RGCs was indispensable. As an experimental animal, the mouse has great advantages not only because it is less expensive and more easily handled than other animals but also because of the availability of various knockout or transgenic mice, enabling investigation of the role of a molecule in vivo. Until now, however, a technique allowing in vivo, noninvasive, and longitudinal observation of RGCs in the living mouse has not been established.

In the present study, we report a method of noninvasive visualization and quantitation of RGCs using B6.Cg-Tg(Thy1-CFP)23Jrs/J[8] mice. The strain expresses cyan fluorescent protein (CFP; major excitation peak, 433 nm; major emission peak, 475 nm),[9] in RGCs under the control of neuron-specific elements from the *Thy1* gene.[8] We evaluated longitudinal changes in the number of RGCs in the living mouse that underwent retinal ischemia reperfusion.[7]

Materials and Methods

Retinal Camera System

We used a commercially available mydriatic retinal camera (TRC-50IX; Topcon, Tokyo, Japan) attached with a 5 million-pixel digital camera (Nikon D1x; Nikon, Tokyo, Japan). The settings of the retinal camera were as follows: pupil, normal; image angle, 50°; flash, 300. The settings of the digital camera were as follows: shutter speed, 1/30 second; ISO, 800; image quality, fine. A 40-diopter aspherical lens (40D; Volk Optical, Mentor, OH) was fixed in front of the objective lens of the retinal camera at a distance of 5 mm, and the optical axis was adjusted. Built-in filters for fluorescein angiography were used for the fluorescein angiogram, band-pass filters, D436/20x (center wavelength, 436 nm; full width at half maximum [FWHM] transmission, 20 nm; Chroma Technology, Rockingham, VT), and BI0049 (center wavelength, 494 nm; FWHM transmission, 33 nm; Asahi Spectra, Tokyo, Japan) were used for the detection of CFP fluorescence. All images were captured with software (IMAGEnet; Topcon) and were saved by 3008 × 1960 × 8 bit-tagged image file format (TIFF). To improve the signal-to-noise ratio, a series of three images was taken for each measurement. The images were aligned automatically (AutoDeblur; Media-Cybernetics, Silver Spring, MD) and were combined (MaxIm DL 4.0; Diffraction Limited, Ontario, BC, Canada).

Ocular Fundus Photography

Three microliters of ophthalmic solution containing 0.5% tropicamide and 0.5% phenylephrine hydrochloride (Mydrin-P; Santen Pharmaceu-

From the [1]Tokyo Metropolitan Geriatric Hospital, Tokyo, Japan; and the [2]Department of Ophthalmology, University of Tokyo School of Medicine, Tokyo, Japan.

Supported in part by Grant H18-Kankakuippan-001 from the Ministry of Health, Labor, and Welfare of Japan and by Grant A18209053 from the Ministry of Education, Culture, Sports, Science and Technology of Japan (MAr).

Submitted for publication September 16, 2007; revised January 6, March 6, and June 25, 2008; accepted October 21, 2008.

Disclosure: **H. Murata**, None; **M. Aihara**, None; **Y.-N. Chen**, None; **T. Ota**, None; **J. Numaga**, None; **M. Araie**, None

The publication costs of this article were defrayed in part by page charge payment. This article must therefore be marked "*advertisement*" in accordance with 18 U.S.C. §1734 solely to indicate this fact.

Corresponding author: Makoto Aihara, Department of Ophthalmology, University of Tokyo School of Medicine, 7-3-1 Hongo, Bunkyo-ku Tokyo 113-8655, Japan; aihara-tky@umin.ac.jp.

Investigative Ophthalmology & Visual Science, December 2008, Vol. 49, No. 12

tical, Osaka, Japan) was applied topically 10 minutes before anesthesia to dilate the pupil, and then mice were anesthetized with intraperitoneal injection of a mixture of ketamine (100 mg/kg body weight) and xylazine (9 mg/kg body weight). To avoid corneal injury, mice were restrained manually until they were anesthetized. A few minutes later, the mice were confirmed by the disappearance of the ciliary reflex to be fully anesthetized, and the cornea was covered carefully with mineral oil (Johnson's Baby Oil; Johnson & Johnson, New Brunswick, NJ) to prevent desiccation and to keep the surface smooth. Smoothness of the corneal surface and transparency were confirmed under an operation microscope. The laterality of the recorded eyes was chosen randomly. All the images were taken by an experienced investigator (HM).

Fluorescein Angiography

A 12-week-old C57BL/6 mouse was used. Ten microliters of fluorescein sodium (10% Fluorescite; Alcon Japan, Tokyo, Japan) was injected into the tail vein, and angiograms were obtained after 5 minutes. Fundus images were obtained using the retinal camera system, as described.

Animal Husbandry

Adult male and female B6.Cg-Tg(Thy1-CFP)23Jrs/J mice[8] were obtained from the breeding colony of The Jackson Laboratory (Bar Harbor, ME). The environment was kept at 23°C with a 12-hour light/12-hour dark cycle. All mice were fed ad libitum. Ten- to 15-week-old mice weighing 20 to 30 g were used. All studies were in compliance with the ARVO Statement for the Use of Animals in Ophthalmic and Vision Research.

Retrograde Labeling of RGCs in the Untreated Group and the Ischemia Reperfusion Group

To investigate the distribution of CFP in the retina, retrograde labeling with 1,1'-dioctadecyl-3,3,3',3'-tetramethylindocarbocyanine perchlorate (DiI) was performed. Three B6.Cg-Tg (Thy1-CFP)23Jrs/J[8] mice were anesthetized and placed in a stereotactic frame. The skull was exposed and kept dry. Two holes were made at 2.92 mm behind the bregma in the anteroposterior axis and 0.5 mm lateral to the midline, and 5% DiI (1 μL at a rate of 0.5 μL/min; Molecular Probes, Eugene, OR) in dimethyl sulfoxide was injected at a depth of 2 mm from the brain surface into the superior colliculus of both sides. Ten days after injection, the mice were killed, and each eye was enucleated and fixed immediately in 4% paraformaldehyde in 0.1 M phosphate-buffered saline (PBS) for 30 minutes at 4°C. After the cornea and lens were removed, the sample was fixed again for 2 hours. Four radial relaxing incisions were made, the retina was prepared as a flattened whole mount on a glass slide with a coverslip, and an image was obtained with a fluorescence microscope (BX50; Olympus, Tokyo, Japan) with appropriate filters. Four square areas of 370 × 370 μm at a distance of approximately 1.5 mm from the optic nerve head were selected, and the number of cells was counted manually by an experienced investigator (MAi). Results were averaged for the four quadrant areas to obtain a value representing the eyes in question.

The same procedure was performed in the ischemia reperfusion group. Three weeks after ischemia reperfusion injury, DiI was injected into five mice of the ischemia reperfusion injury group. Seven days after injection, the retina was whole mounted. Then DiI^+ cells among CFP-expressing cells and CFP^+ cells among DiI^+ cells were counted and compared with those in untreated control eyes by an unpaired *t*-test. $P < 0.05$ was considered statistically significant.

Frozen Section

Localization of CFP^+ cells in the retina was assessed by retinal frozen sections. Four eyes of two thy1-CFP mice were enucleated, fixed in 4% paraformaldehyde in 0.1 M PBS for 1 hour, and fixed again for 1 hour after the removal of the cornea and lens. The globes were embedded (Tissue-Tek O.C.T.; Sakura Finetechnical, Tokyo, Japan) and cryopreserved in 15-mm-thick frozen sections, and sequential meridian sections (5-μm thick) were made through the optic disc. Sections were mounted on a glass slide with antifade medium containing propidium iodide (VectaShield with propidium iodide H-1300: Vector Laboratories, Burlingame, CA) to stain nuclei.

Comparison of a Mouse Fundus Photograph with a Whole Mount Retinal Image

Immediately after fundus photographs were obtained from a B6.Cg-Tg (Thy1-CFP) 23Jrs/J mouse,[8] the mouse was killed, and the retina was whole mounted and photographed with a fluorescence microscope (MZFLIII; Leica Microsystems Japan, Tokyo, Japan).

Ischemia Reperfusion Injury

Five mice were used for the ischemia reperfusion injury model.[10] Sodium pentobarbital (50 mg/kg body weight) was administered intraperitoneally. After anesthesia, the anterior chamber of the right eye was cannulated with a microneedle[11] connected to a reservoir filled with intraocular irrigating solution (BSS Plus; Santen Pharmaceutical). Retinal ischemia was induced by elevating the reservoir, and the IOP was raised to 110 mm Hg for 60 minutes.[12] During ischemia, the IOP was monitored continuously, the room temperature was maintained at 25°C,[13] and the room was kept dark. Ocular fundus images were recorded as described at five time points, just before injury and 1, 2, 3, and 4 weeks after it. Seven mice underwent sham operation by cannulation of the microneedle without elevation of the intracameral pressure and were used as controls. Their retinal images were recorded five times at 1-week intervals.

Reproducibility of Counting and Regional Difference of the Number of RGCs

We took fundus photographs of 10 eyes of five mice. Bilateral eyes of each mouse underwent fundus photography twice at intervals of 24 hours. The number of RGCs in the same area of the four square fields (220 × 220 pixels) was counted manually. Moreover, cell density was counted in each of four areas to investigate the regional differences of sampled area in each quadrant located 800 μm apart from the optic disc.

RGC Counting in Fundus Photographs and Retinal Flat Mount

Four square fields of 220 × 220 pixels (approximately 370 × 370 μm), one field from each quadrant of the retina, at a distance of approximately 800 μm from the optic nerve disc was always used for RGC counting in the fundus photograph or retinal flat mount, respectively. The number of cells emitting fluorescence was counted manually. Cell counting was performed by an experienced investigator (MAi) who was masked to the experimental treatment of the eye.

The numbers of RGCs counted in four square fields in the retina of ischemia reperfusion eyes were normalized to those obtained identically in the control eyes and were indicated as RGC survival rate. Each percentage is expressed in the text and figures as the mean ± SD. The difference in RGC density among four areas was statistically analyzed by a Kruskal-Wallis test. $P < 0.05$ was considered statistically significant.

Histologic Evaluation

After the last fundus photograph was taken at 4 weeks, one mouse was chosen randomly from the sham-operated control group and the ischemia reperfusion injury group. The mice were killed, and their eyes were enucleated, fixed in 4% paraformaldehyde and 2.5% glutaraldehyde in 0.1 M PBS for 1 hour, and fixed again for 24 hours after removal of the cornea and lens. The globes were processed to paraffin-embedded sections, and sequential meridian sections (5-μm thick) were made through the optic disc. Sections were stained with hematoxylin and eosin. Sections were examined with a light microscope (BX50; Olympus).

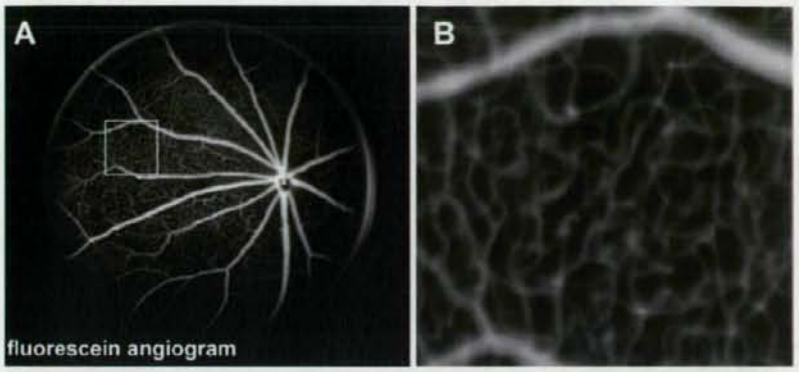

FIGURE 1. (**A**) Fluorescein angiogram of the mouse ocular fundus. (**B**) Area corresponding area to the *insert* in (**A**).

RESULTS

Mouse Fundus Photography

At first, to examine the resolving power of the fundus photograph with our method, we took a fundus fluorescein angiogram of a C57BL/6J mouse (Figs. 1A, 1B).

A wide area of retina was recorded, and blood capillaries were visualized with sufficient quality. Comparison of the fluorescein angiogram with those obtained from other studies suggested that the resolving power provided by our system was similar to that provided by a 10° view of a confocal scanning laser ophthalmoscope (cSLO) and superior to a 20° view of it,[14–16] whereas the area recorded by our system was similar to that provided by a 20° view of a cSLO.

Investigation of CFP Expression in the Mouse Retina

To identify the distribution of CFP in the B6.Cg-Tg(Thy1-CFP)23Jrs/J[18] mouse retina, retrograde labeling of RGCs with DiI was performed in five untreated eyes of three mice. Colo-

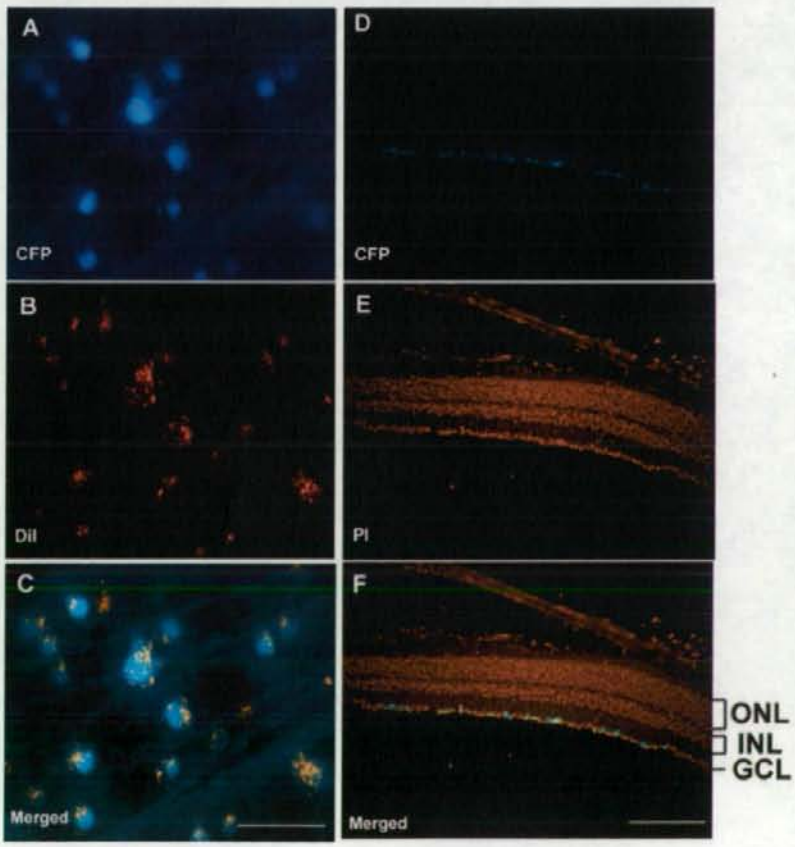

FIGURE 2. (**A–C**) Double labeling of RGCs with CFP and DiI. (**A**) RGCs expressing CFP. (**B**) Same field of DiI optics. (**C**) Merged image of (**A**) and (**B**). (**D–F**) Frozen section of Thy-1 CFP mouse. CFP was expressed only in the ganglion cell layer. Scale bars, (**A–C**) 50 μm; (**D–F**) 200 μm.

TABLE 1. Types of Labeling with CFP and DiI in Ischemia Reperfusion Group and Control Group

Cells	Control (%)	Ischemia Reperfusion (%)
DiI^+ among CFP^+	97.0	97.8
DiI^- among CFP^+	3.0	2.2
CFP^+ among DiI^+	72.6	59.2
CFP^- among DiI^+	27.4	40.8

calization of CFP and DiI in the same cells was observed (Figs. 2A–2C). Among the CFP^+ cells, DiI^+ cells accounted for 97.0% ± 2.7% (mean ± SD, $n = 5$) and DiI^- cells accounted for 3.0% ± 2.7%. Among the DiI^+ cells, CFP^+ cells accounted for 72.6% ± 5.2%, and CFP^- cells accounted for 27.4% ± 5.2% (Table 1). The density of DiI^+ cells was 2100 ± 136 cells/μm^2. Figures 2D–2F indicated that all the CFP^+ cells were localized only in the RGC layer.

Visualization of RGCs In Vivo and Comparison of a Fundus Photograph with a Whole Mount Retinal Image

Clear fundus images could be obtained routinely under anesthesia, and mouse RGCs could be identified in vivo at the single-cell level.

By postural change, the superior, inferior, temporal, nasal, and central retina could be visualized. It was difficult, however, to take a photograph of the same living mouse and to achieve acceptable image quality in the peripheral retina, more than 1200 μm from optic disc, or even in the central retina in mice younger than 8 weeks or in those with corneal opacity.

Given that the mice were breathing during ocular fundus photography, a short exposure time was desirable to acquire clearer images without motion blur. However, short exposure time reduces the quality of the images, which was managed by combining three images. Because acute development of lens opacity is frequently encountered under general anesthesia in mice[17] and the pupil diameter of mice is smaller than that of rats, the image quality of mouse fundus photography had been limited. Covering the cornea with mineral oil not only keeps its surface smooth, it prevents the development of lens opacity. The excitation light was concentrated by a 40-D lens to pass small pupils.

To measure the resolution of ocular fundus photography, we compared the fundus photographs (Figs. 3A, 3B) and the images of the whole mount retina (Fig. 3C). This revealed that one pixel in a fundus photograph corresponded to a square of approximately 1.7 × 1.7 μm. The image of RGCs in the fundus photographs showed excellent concordance with that in the whole mount retina (Figs. 3B, 3C).

To verify that longitudinal recording of fundus photographs could be achieved with our methods, we took fundus photographs twice at intervals of 1 week and compared them. Even a single-cell loss could be visualized by our methods (Figs. 3D, 3E).

Reproducibility of Counting the Number of RGCs

To examine reproducibility, we took fundus photographs twice at intervals of 24 hours and counted RGCs manually in the same field of the four square fields, and then we calculated the intraclass correlation (ICC) and the coefficient of variation (CV) between the results obtained from the first and second photographs. The numbers of RGCs in the selected square field (220 × 220 pixels) were 187 ± 21 and 184 ± 22 (mean ± SD; $n = 10$) in the first and second photographs, respectively, the ICC was 0.941, and the CV was 2.1% ± 2.4% (mean ± SD). The density of RGCs in the four areas from nasal, superior, temporal, and inferior quadrants of the central retina were 1505 ± 89/mm^2, 1386 ± 111/mm^2, 1593 ± 139/mm^2, and 1563 ± 68/mm^2, respectively (Table 2). Among each of four areas, no statistical difference in the density of RGCs was seen (Kruskal-Wallis test; $P = 0.054$).

Longitudinal Evaluation of RGCs in Ischemia Reperfusion Models

We recorded fundus photographs longitudinally in the ischemia reperfusion model group and the sham-operated control group to evaluate the longitudinal changes in the number of RGCs in this experimental model. Figures 4A–4J indicate the longitudinal change in the RGC image in one eye after ischemia

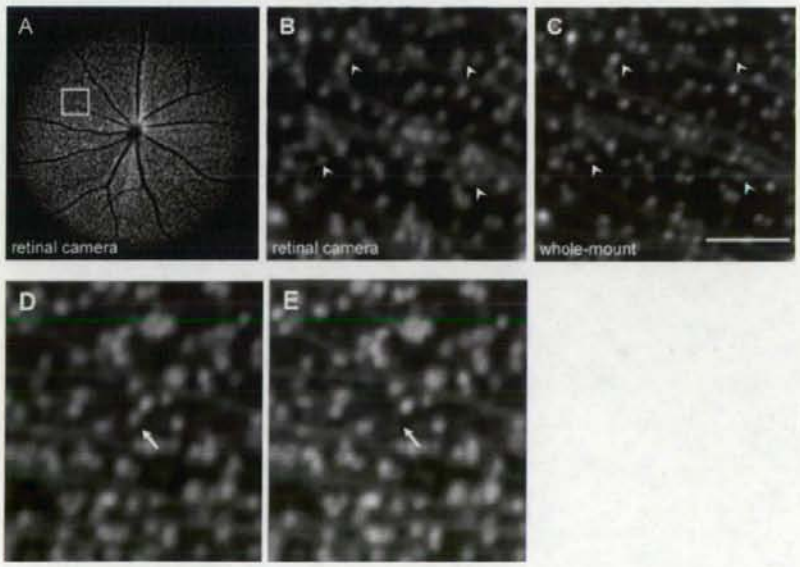

FIGURE 3. (**A**) Representative examples of mouse ocular fundus photographs. (**B**, **C**) Fundus photographs and whole mount of retina corresponding to the *insert* in (**A**). (**B**, **C**, *arrowheads*) Corresponding location. (**D**, **E**) RGC loss (*white arrow*) in the control eye could be detected clearly with our method. Scale bar, 100 μm.

TABLE 2. Density of CFP-Expressing RGCs (cells/mm^2) in the Four Areas of the Retina

	Mouse					
Area	1	2	3	4	5	Mean ± SD
Nasal	1525	1637	1511	1401	1449	1505 ± 89
Superior	1285	1381	1527	1271	1462	1386 ± 111
Inferior	1649	1402	1609	1527	1776	1593 ± 139
Temporal	1615	1583	1625	1461	1530	1563 ± 68

reperfusion injury, and Figures 4K and 4L indicate longitudinal change in that the control group.

Reduction of RGC numbers was evaluated sequentially in the same eyes. The number of RGCs and the fluorescence intensity of the nerve fiber decreased considerably during the first week. The percentages of RGCs decreased to 34.2% ± 7.5%, 24.1% ± 9.1%, 23.0% ± 9.3%, and 22.2% ± 8.4% (mean ± SD; $n = 5$) of the percentages before injury at 1, 2, 3, and 4 weeks after the injury, respectively ($P < 0.001$).

The percentages of RGCs in the control eyes were unchanged: 100.5% ± 4.1%, 100.4% ± 3.5%, 101.4% ± 2.3%, and 100.0% ± 3.0% (mean ± SD, $n = 7$) of the percentages before sham operation at 1, 2, 3, and 4 weeks, respectively. The percentages of RGCs with CFP fluorescence after injury to that before injury is shown in Figure 4M.

Histopathologic Evaluation

Figures 5A and 5B show a retinal section of a sham-operated control eye and of that of a treated eye 4 weeks after ischemia reperfusion injury, respectively.

The thickness of the RGC layer and the number of RGCs were markedly reduced in the ischemia reperfusion injury. Moreover, the thickness of the inner plexiform layer was reduced considerably in the ischemia reperfusion injury group

Figures 5C–5E indicate the retrogradely labeled RGCs with DiI in an eye of the ischemia reperfusion injury group in the whole mount retina 4 weeks after injury. In the ischemia reperfusion injury group, DiI$^+$ cells constituted 97.8% ± 3.1% (mean ± SD, five eyes of five mice) and DiI$^-$ cells constituted 2.2% ± 3.1% of the CFP$^+$ cells. Among the DiI$^+$ cells, CFP$^+$ cells constituted

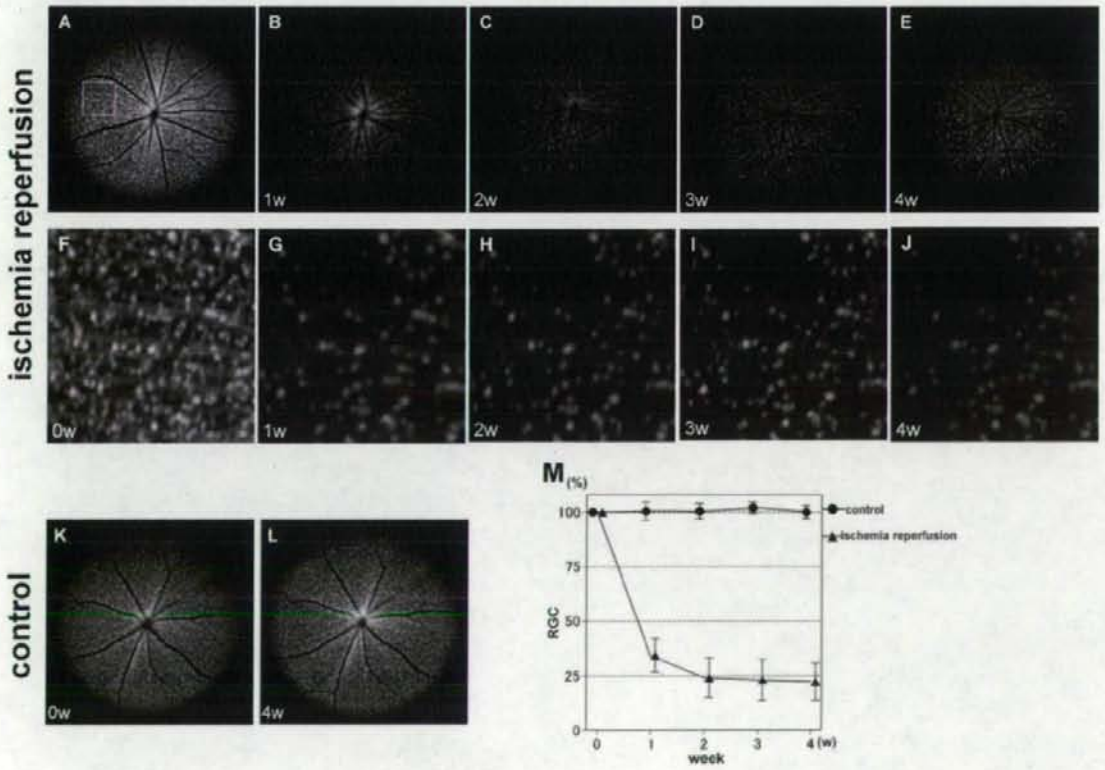

FIGURE 4. Longitudinal evaluation of the ischemia reperfusion injury model group. (**A**, **F**) Presurgery. (**B**, **G**) 1, (**C**, **H**) 2, (**D**, **I**) 3, and (**E**, **J**) 4 weeks after injury. (**F**–**J**) Corresponding area to the *insert* in (**A**). (**K**, **L**) Longitudinal evaluation of the control group. (**M**) Longitudinal changes of RGCs. The survival ratio of RGCs in postoperative period against that in the preoperative period in the control group ($n = 7$, *circles*) and the ischemia reperfusion injury model group ($n = 5$, *triangles*). Error bars indicate SD.

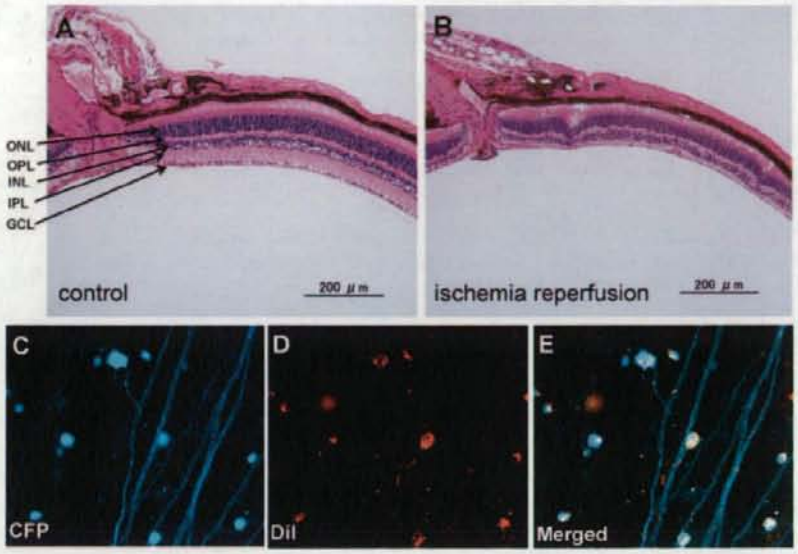

FIGURE 5. (A, B) Histologic evaluation of paraffin-embedded, hematoxylin/eosin-stained retinal sections. (A) Four weeks after sham operation and (B) 4 weeks after ischemia reperfusion injury. GCL, ganglion cell layer; IPL, inner plexiform layer; INL, inner nuclear layer; OPL, outer plexiform layer; ONL, outer nuclear layer. (C–E) Whole mount retina 4 weeks after ischemia reperfusion injury. Scale bars, 100 μm.

59.2% ± 3.4% and CFP$^-$ cells constituted 40.8% ± 3.4% (Figs. 5C–E; Table 1). The percentage of the CFP$^+$ cells among the DiI$^+$ cells in the ischemia reperfusion injury group was significantly less than that in the control group ($P = 0.03$ by unpaired t-test; 59.2% ± 3.4% vs. 72.6% ± 5.2%).

DISCUSSION

Experimental mouse models are often applied to investigate the pathophysiology of human diseases. In vivo observation of apoptotic RGCs labeled with intravitreously injected Annexin V[18] and of retrogradely labeled RGCs after injection of a fluorescent dye into the superior colliculus[19] were reported in a rat model. Annexin V can bind to externalized phosphatidylserine, reflecting a preapoptotic condition,[18] but intravitreous injection may limit the experimental protocols and affect outcomes. Moreover, longitudinal counting of apoptotic RGCs was not performed in that study.[18] Fluorochromes such as DiA, DiI, and 4Di-10-ASP have often been used for labeling RGCs, but injection of exogenous dye into the superior colliculus is required, and sometimes RGCs are not labeled uniformly. Frequently used neurotracers are relatively stable, and microglia can be labeled secondarily by phagocytosing degenerated RGCs.[19,20] Lastly, genetic modification and experimental tools are less available in the rat than in the mouse.

Feng et al.[8] recently developed transgenic mice expressing CFP in living RGCs, which allowed us to visualize RGCs histologically. This mouse also paves the way for noninvasive observation of living RGCs in vivo. One of the benefits of the transgenic mouse is that it enables more precise cell counting than does the mouse with retrogradely labeled RGCs because CFP expression in the cytosol could delineate the cell body of RGCs whereas DiI is detected as particles in the RGC cytosol. Thus, some overlaid or adjacent cells were distinguished easily by the margin of CFP-stained cytosol (Figs. 2A–2C). Although our method relied on manual counting of CFP-stained RGCs as previous retrograde labeling method,[19] reproducibility of the result given by a masked, experienced investigator was thought to be sufficiently high.

In our devices, a pixel in the fundus photograph corresponds to approximately 1.7 × 1.7 μm, and an RGC soma measures 5 μm or more.[21] Thus, theoretically our system has sufficient resolution to detect an individual RGC. Comparison of ocular fundus images and the whole mount retina of the same eye confirmed that our method could capture almost all RGCs expressing CFP (Figs. 3B, 3C), and even the loss of a single cell could be detected with our method (Figs. 3D, 3E).

Available methods to evaluate experimental neurodegeneration by counting RGCs in the whole mount retina[22] or by measuring the thickness of retinal sections[12] require a large number of experimental animals and are limited in their ability to detect subtle changes in RGCs. We could detect RGC reduction with a smaller number of mice without sacrificing them by in vivo sequential imaging of the same region in a single eye.

Ocular fundus images of mice have been obtained in two ways: by means of a retinal camera[23] (a conventional method of fundus photography) and by cSLO.[14–16,24,25] In cSLO, the obtained image measures only 768 × 768 pixels,[26] and the detectable fluorescence is limited because of the limitation of available wavelength for excitation light (460 nm, 488 nm, 514 nm, 795 nm, and 830 nm).[14,25] Although these reports do not clearly mention the actual image area taken by one shot, montage photographs or several shots are required to evaluate a sufficiently wide area of the retina. On the other hand, approximately 25% of the whole RGCs (1700 × 1700 μm) can be longitudinally photographed in the same area of the same retina as one image by our method with a retinal camera. Moreover, a retinal camera, which is more cost-effective than cSLO, can support the use of various fluorescent dyes by changing fluorescence filters. One of the limitations is that RGCs in the peripheral retina 1200 μm or more apart from the disc could not be evaluated by our method because of the difficulty of taking images of acceptable quality. Thus, approximately central 36% of the whole area of the retina can be evaluated by the current method. This limitation that the whole retina could not be evaluated by our in vivo fundus photography also applied to the methods of in vivo imaging with Annexin V staining[18] or of scanning laser ophthalmoscopy.[19] In addition, it is challenging to take retinal photographs of mouse eyes younger than 8 weeks of age or with corneal opacity.

B6.Cg-Tg(Thy1-CFP)23Jrs/J mice express CFP in some amacrine cells, and all RGCs do not always express CFP.[18] Thus, with our method, some amacrine cells may be co-counted as a total number, but some RGCs may not be counted. However, CFP^+ and DiI^- cells, which are considered to be CFP^+ amacrine cells, were only 3% of the total CFP^+ cells, and CFP^+ and DiI^+ cells, which are considered to be CFP^+ RGCs, were approximately 73% of the total DiI^+ cells. Thus, any amacrine cells included should have only a minor effect on the RGC count.

One intriguing finding is that the percentage of CFP^+ cells among the DiI^+ cells in ischemia-reperfusion group 4 weeks after injury was significantly lower than that in the untreated group (59.2% vs. 72.6%). It was reported previously that $Thy1^+$ RGCs decrease rapidly after injury,[27,28] and Thy1 is a more sensitive marker of injured RGCs.[29] In our system, CFP^+ cells are thought to reflect $Thy1^+$ cells indirectly because the expression of CFP and Thy1 is linked genetically in this transgenic mouse. Thus, CFP^- RGCs after injury may reflect dysfunction of a basic cellular activity, gene transcription. On the other hand, DiI or other imported particles do not reflect cellular activity, even though they are observed in the cell body, because they can remain in the cells as long as the cell structure is conserved. In fact, our study indicated that injured RGCs after ischemia reperfusion detected by CFP fluorescent fadeaway progressed earlier than they did in other studies.[15] Thus, our system using CFP expression linked with Thy1 to detect cell injury may have advantages in the sensitivity to detect the earlier changes of cell death compared with other labeling methods.

In vivo imaging in neurodegenerative mouse models has many advantages.[30] By using our method to evaluate the number of RGCs longitudinally in the same animals, it is possible to monitor the time course of RGC injury or neuroprotective effects of drugs. Moreover, cross-breeding of various genetically modified mice and CFP-expressing mice would have great potential in investigating the time course of RGC death. Our technique may open up the possibility of detailed investigations of neurodegeneration or nerve regeneration through mouse eyes.

Acknowledgments

The authors thank Aya Iriyama and Masaaki Ohashi for histologic evaluation.

References

1. Burgoyne CF. Image analysis of optic nerve disease. *Eye.* 2004;18:1207–1213.
2. Fujimoto JG. Optical coherence tomography for ultrahigh resolution in vivo imaging. *Nat Biotechnol.* 2003;21:1361–1367.
3. Quigley HA. Number of people with glaucoma worldwide. *Br J Ophthalmol.* 1996;80:389–393.
4. Clark AF, Yorio T. Ophthalmic drug discovery. *Nat Rev Drug Discov.* 2003;2:448–459.
5. Goldberg I. Relationship between intraocular pressure and preservation of visual field in glaucoma. *Surv Ophthalmol.* 2003;48(suppl 1):S3–S7.
6. Fechtner RD, Weinreb RN. Mechanisms of optic nerve damage in primary open angle glaucoma. *Surv Ophthalmol.* 1994;39:23–42.
7. Goldblum D, Mittag T. Prospects for relevant glaucoma models with retinal ganglion cell damage in the rodent eye. *Vision Res.* 2002;42:471–478.
8. Feng G, Mellor RH, Bernstein M, et al. Imaging neuronal subsets in transgenic mice expressing multiple spectral variants of GFP. *Neuron.* 2000;28:41–51.
9. Shaner NC, Steinbach PA, Tsien RY. A guide to choosing fluorescent proteins. *Nat Methods.* 2005;2:905–909.
10. Harada C, Harada T, Slusher BS, Yoshida K, Matsuda H, Wada K. N-acetylated-alpha-linked-acidic dipeptidase inhibitor has a neuroprotective effect on mouse retinal ganglion cells after pressure-induced ischemia. *Neurosci Lett.* 2000;292:134–136.
11. Aihara M, Lindsey JD, Weinreb RN. Reduction of intraocular pressure in mouse eyes treated with latanoprost. *Invest Ophthalmol Vis Sci.* 2002;43:146–150.
12. Lam TT, Abler AS, Tso MO. Apoptosis and caspases after ischemia-reperfusion injury in rat retina. *Invest Ophthalmol Vis Sci.* 1999;40:967–975.
13. Lafuente MP, Villegas-Perez MP, Selles-Navarro I, et al. Retinal ganglion cell death after acute retinal ischemia is an ongoing process whose severity and duration depends on the duration of the insult. *Neuroscience.* 2002;109:157–168.
14. Sceliger MW, Beck SC, Pereyra-Munoz N, et al. In vivo confocal imaging of the retina in animal models using scanning laser ophthalmoscopy. *Vision Res.* 2005;45:3512–3519.
15. Luhmann UF, Lin J, Acar N, et al. Role of the Norrie disease pseudoglioma gene in sprouting angiogenesis during development of the retinal vasculature. *Invest Ophthalmol Vis Sci.* 2005;46:3372–3382.
16. Paques M, Simonutti M, Roux MJ, et al. High resolution fundus imaging by confocal scanning laser ophthalmoscopy in the mouse. *Vision Res.* 2006;46:1336–1345.
17. Calderone L, Grimes P, Shalev M. Acute reversible cataract induced by xylazine and by ketamine-xylazine anesthesia in rats and mice. *Exp Eye Res.* 1986;42:331–337.
18. Cordeiro MF, Guo L, Luong V, et al. Real-time imaging of single nerve cell apoptosis in retinal neurodegeneration. *Proc Natl Acad Sci U S A.* 2004;101:13352–13356.
19. Higashide T, Kawaguchi I, Ohkubo S, Takeda H, Sugiyama K. In vivo imaging and counting of rat retinal ganglion cells using a scanning laser ophthalmoscope. *Invest Ophthalmol Vis Sci.* 2006;47:2943–2950.
20. Thanos S, Kacza J, Seeger J, Mey J. Old dyes for new scopes: the phagocytosis-dependent long-term fluorescence labelling of microglial cells in vivo. *Trends Neurosci.* 1994;17:177–182.
21. Perry VH. Evidence for an amacrine cell system in the ganglion cell layer of the rat retina. *Neuroscience.* 1981;6:931–944.
22. Inoue T, Hosokawa M, Morigiwa K, Ohashi Y, Fukuda Y. Bcl-2 overexpression does not enhance in vivo axonal regeneration of retinal ganglion cells after peripheral nerve transplantation in adult mice. *J Neurosci.* 2002;22:4468–4477.
23. Hawes NL, Smith RS, Chang B, Davisson M, Heckenlively JR, John SW. Mouse fundus photography and angiography: a catalogue of normal and mutant phenotypes. *Mol Vis.* 1999;5:22.
24. Jaissle GB, May CA, Reinhard J, et al. Evaluation of the rhodopsin knockout mouse as a model of pure cone function. *Invest Ophthalmol Vis Sci.* 2001;42:506–513.
25. Leung CK, Lindsey JD, Crowston JG, et al. In vivo imaging of murine retinal ganglion cells. *J Neurosci Methods.* 2008;168:475–478.
26. Jorzik JJ, Bindewald A, Dithmar S, Holz FG. Digital simultaneous fluorescein and indocyanine green angiography, autofluorescence, and red-free imaging with a solid-state laser-based confocal scanning laser ophthalmoscope. *Retina.* 2005;25:405–416.
27. Schlamp CL, Johnson EC, Li Y, Morrison JC, Nickells RW. Changes in Thy1 gene expression associated with damaged retinal ganglion cells. *Mol Vis.* 2001;7:192–201.
28. Huang W, Fileta J, Guo Y, Grosskreutz CL. Downregulation of Thy1 in retinal ganglion cells in experimental glaucoma. *Curr Eye Res.* 2006;31:265–271.
29. Chidlow G, Casson R, Sobrado-Calvo P, Vidal-Sanz M, Osborne NN. Measurement of retinal injury in the rat after optic nerve transection: an RT-PCR study. *Mol Vis.* 2005;11:387–396.
30. Misgeld T, Kerschensteiner M. In vivo imaging of the diseased nervous system. *Nat Rev Neurosci.* 2006;7:449–463.